

Dynamics and Variability of the Spring Dry Season in the United States Southwest as Observed in AmeriFlux and NLDAS-2 Data

MADELEINE PASCOLINI-CAMPBELL^a

Columbia University, New York City, New York

RICHARD SEAGER AND A. PARK WILLIAMS

Lamont-Doherty Earth Observatory, Palisades, New York

BENJAMIN I. COOK

NASA Goddard Institute for Space Studies, New York, New York

ARIANE O. PINSON

Albuquerque District, U.S. Army Corps of Engineers, Albuquerque, New Mexico

(Manuscript received 25 July 2018, in final form 27 March 2019)

ABSTRACT

The spring dry season occurring in an arid region of the southwestern United States, which receives both winter storm track and summer monsoon precipitation, is investigated. Bimodal precipitation and vegetation growth provide an opportunity to assess multiple climate mechanisms and their impact on hydroclimate and ecosystems. We detect multiple shifts from wet to drier conditions in the observational record and land surface model output. Focusing on the recent dry period, a shift in the late 1990s resulted in earlier and greater spring soil moisture draw down, and later and reduced spring vegetation green-up, compared to a prior wet period (1979–97). A simple soil moisture balance model shows this shift is driven by changes in winter precipitation. The recent post-1999 dry period and an earlier one from 1948 to 1966 are both related to the cool tropics phase of Pacific decadal variability, which influences winter precipitation. In agreement with other studies for the southwestern United States, we find the recent drought cannot be explained in terms of precipitation alone, but also is due to the rising influence of temperature, thus highlighting the sensitivity of this region to warming temperatures. Future changes in the spring dry season will therefore be affected by how tropical decadal variability evolves, and also by emerging trends due to human-driven warming.

1. Introduction

There is a region of the interior southwestern United States (SWUS) that has two seasons of precipitation: one from the winter storm track and one from the North American summer monsoon (NAM). Subsequently, this region undergoes two periods of vegetation green-up in the early spring and summer (Adams and Comrie 1997;

Guirguis and Avissar 2008), with a dry season occurring throughout the intervening spring months when ecosystem productivity declines. This area is also influenced by modes of climate variability associated with Pacific sea surface temperature (SST) on interannual to interdecadal time scales. Furthermore, the SWUS has undergone warming during the twentieth-century (Hoerling et al. 2013), and the most recent twenty-first century drought in the SWUS has already contributed to vegetation die-off (Breshears et al. 2005). As yet, no studies have explicitly investigated how the intervening spring dry season responds to both natural climate variability and warming in this region of two-peak greening. Given the close coupling between climate and vegetation, and the overall sensitivity of the

^a Current affiliation: Jet Propulsion Laboratory, California Institute of Technology, Pasadena, California.

Corresponding author: Madeleine Pascolini-Campbell, map2251@columbia.edu

SWUS to future anthropogenic climate change, this study aims to investigate past and present dynamics of the unique ecohydrology of this region.

On a year-to-year basis, the mechanisms producing bimodal vegetation green-up in the region have been studied using observations and models, and are as follows. Winter precipitation and snowmelt add water to the soils, which is then gradually drawn down by vegetation growth and rising spring temperatures, leading to enhanced ET (Kurc and Small 2007; Vivoni et al. 2008). Vegetation greening reaches its spring peak, and then declines with soil moisture over the course of the spring dry season, until the arrival of the NAM, which creates a new pulse in soil moisture and vegetation growth. Prior studies using both observations and land surface modeling for the SWUS, have identified the storage of water in soils from winter to spring as being critical to the bimodal seasonal cycle of vegetation green-up, while the summer green-up is concurrent with the NAM (Notaro et al. 2010; Muldavin et al. 2008). Summer vegetation greening and soil moisture are closely related to the magnitude of NAM, and produce important feedbacks with the atmosphere via enhanced ET (Matsui et al. 2005; Notaro and Gutzler 2012). In either case, water availability exerts the dominant control on ecosystem productivity in the SWUS (Huxman et al. 2004; Scott et al. 2009; Vivoni et al. 2008; Watts et al. 2007). Climate controls on precipitation can therefore influence the timing and intensity of spring and summer greenings, and the intervening spring drying.

The controls on moisture inputs in the region are also well known: a smaller peak in precipitation occurs during the winter in the form of both rain and snow and is largely influenced by the Pacific storm track. The NAM is the dominant source of moisture in the region, delivering a large amount of precipitation as rain during the summer months (Adams and Comrie 1997), which marks the end of the spring dry period. In addition to internal atmosphere variability, year-to-year variations in winter precipitation are modulated by tropical Pacific SSTs. These teleconnections are well documented, with El Niño–Southern Oscillation (ENSO) being the dominant driver interannually (Ropelewski and Halpert 1986, 1989), and the Pacific decadal oscillation (PDO) operating on interdecadal time scales (McCabe et al. 2004). The tropical North Atlantic Ocean also plays a likely role, with cold years favoring above normal precipitation in the SWUS (Enfield et al. 2001). The NAM also varies interannually and has been found to be weakly influenced by phases of ENSO (Higgins et al. 1999; Castro et al. 2001), the Madden–Julian oscillation (MJO) (Higgins and Shi 2001), and soil moisture (Small 2001).

The region is highly sensitive to anthropogenically induced warming. Twentieth-century observations have

indicated an earlier onset of spring in the SWUS, as defined by the timing of blooming and snowmelt, which is primarily attributed to increased spring temperatures (Cayan et al. 2001; Ault 2015). Observations have also suggested a shortening of the NAM in the past four decades due to an earlier retreat of summer precipitation (Arias et al. 2015). The magnitude, timing and melt of the snowpack from winter precipitation influences the storage of water in soils, and observational studies of Snowpack Telemetry (SNOTEL) sites have indicated a trend toward reduced snowpack in the western United States and earlier melt (Mote et al. 2005; Fritze et al. 2011; Mote et al. 2018). Impacts on the SWUS include an earlier dry season, an earlier spring vegetation green-up as well as earlier spring streamflow (Fritze et al. 2011; Hand et al. 2016). An earlier spring dry season also leads to a longer wildfire season (Westerling et al. 2006; Williams et al. 2014) and can enhance dust emissions (Hand et al. 2016).

Modeling studies have projected increased drying in the SWUS due to future reductions in precipitation and increases in potential ET (PET) (Seager et al. 2007; Cook et al. 2015; Seager et al. 2013a), and this drying is particularly robust during the spring (Gao et al. 2014). Analysis of the phase 5 of the Coupled Model Intercomparison Project (CMIP5) ensemble attributed projected spring drying in the SWUS to decreased mean moisture convergence associated with enhanced dry zonal advection (Ting et al. 2018). Other modeling studies have indicated a delayed onset of the NAM, and declines in early season NAM precipitation (Cook and Seager 2013), or overall weakening of the NAM under enhanced greenhouse gas forcing (Pascale et al. 2017). It follows that implications for the dry season would include a longer and more intense spring drying, with resulting ramifications on ecosystems in this sensitive SWUS region. In addition to natural climate variability, assessing the role of warming temperatures on the ecohydrology of the bimodal region is critical in light of these projected changes.

The role of climate variability on ecosystem productivity has been studied in this region (Kurc and Small 2007; Vivoni et al. 2008; Notaro et al. 2010), as well as the effect of warming temperatures (Breshears et al. 2005). In addition, as referenced above, there has been considerable research on the climate variability and change of the winter and summer wet seasons. However, variability and change of climate, hydrology, and ecology of the intervening spring drying has not been explicitly investigated. Given the complex interaction between multiple variables (precipitation, snowmelt, ET, runoff, soil moisture, and vegetation), different moisture inputs (winter storms and NAM), modes of

TABLE 1. Summary of AmeriFlux in situ data.

Site name	Location	Temporal availability	Vegetation	Elevation (m)
U.S.-Valles Caldera Ponderosa Pine (U.S.-Vcp)	35.8°, -106.6°	2007-14	Evergreen needleleaf forest	2500
U.S.-Valles Caldera Mixed Conifer (U.S.-Vcm)	35.8°, -106.5°	2007-14	Evergreen needleleaf forest	3030
U.S.-Flagstaff Managed Forest (U.S.-Fmf)	35.1°, -111.7°	2006-10	Evergreen needleleaf forest	2160
U.S.-Flagstaff Unmanaged Forest (U.S.-Fuf)	35.1°, -111.8°	2006-10	Evergreen needleleaf forest	2180
U.S.-Flagstaff Wildfire (U.S.-Fwf)	35.4°, -111.8°	2006-10	Grasslands	2270
U.S.-Sevilleta grassland (U.S.-Seg)	34.4°, -106.7°	2007-14	Grasslands	1596
U.S.-Sevilleta shrubland (U.S.-Ses)	34.3°, -106.7°	2007-14	Open shrublands	1604
U.S.-Willard Juniper Savannah (U.S.-Wjs)	34.4°, -105.9°	2007-14	Savannah	1931
U.S.-Mountainair Pinyon-Juniper Woodland (U.S.-Mpi)	34.4°, -106.2°	2007-14	Woody savannah	2196
U.S.-Santa Rita Creosote (U.S.-SRC)	31.9°, -110.8°	2008-15	Open shrublands	991
U.S.-Santa Rita Grassland (U.S.-SRG)	31.8°, -110.8°	2008-15	Grasslands	1291
U.S.-Santa Rita Mesquite (U.S.-SRM)	31.8°, -110.8°	2004-15	Woody savannas	1120
U.S.-Walnut Gulch Lucky Hills Shrub (U.S.-Whs)	31.7°, -110.0°	2007-15	Open shrublands	1370
U.S.-Walnut Gulch Kendall Grassland (U.S.-Wkg)	31.7°, -109.9°	2004-15	Grasslands	1531
U.S.-Audubon Research Ranch (U.S.-Aud)	31.6°, -110.5°	2002-15	Grasslands	1469

climate variability (ENSO, PDO), and anthropogenic change, a comprehensive understanding of the climate dynamics required to understand past and projected future change in the ecohydrology of this unique area is needed.

Specifically, in this study, after first providing a description of the climatological ecohydrology of the region based on up-to-date in situ and remotely sensed data, we address the following:

- 1) How has hydroclimate changed on decadal time scales, and how has this influenced the spring and summer vegetation green-ups?
- 2) How do shifts in hydroclimate influence the magnitude, timing, and duration of the intervening spring dry season?
- 3) Is there an influence of warming temperatures on the ecohydrology of the region?

This study will seek to answer these questions using in situ, remotely sensed observations and land surface models (LSMs). Results from this study will identify the key climate mechanisms which influence the climatology, decadal variability and trends in spring drying in this region, and provide a background for what to expect under future climate change. Results will also be used to inform what the implications of climate change and continued anthropogenic warming are for ecosystems in the region.

2. Data and methods

To examine the characteristics at the site level we use in situ observations from the AmeriFlux network. For a broader study of the dual season region over a longer

time period, we examine data from LSMs forced by gridded meteorological data.

The in situ observations of precipitation, net ecosystem productivity (NEP), latent heat flux, and soil water content are obtained from the AmeriFlux network for different sites in the SWUS (available online at <http://ameriflux.lbl.gov>), and their location, climate, and temporal availability are listed in Table 1. The AmeriFlux network uses eddy covariance methods to make half-hourly temporal resolution estimates of the fluxes of ecosystem CO₂, water, and energy in North America (Baldocchi et al. 2001).

Given the limited temporal and spatial coverage of the AmeriFlux sites, we also use output from the second phase of the National Land Data Assimilation system (NLDAS-2) LSMs Noah, Mosaic, and VIC for soil moisture, ET, snowmelt, snowfall, and total runoff (surface plus subsurface) at 1/8° resolution (Xia et al. 2012; available online at <https://ldas.gsfc.nasa.gov/nldas/>; Table 2). The LSMs do not have dynamic vegetation, and the annual cycle of the leaf area index (LAI) is prescribed. The LSM data are available from 1979 to present at hourly temporal resolution. Each of the three LSMs is forced with Climate Prediction Center unified gauge-based precipitation data with Parameter-Elevation Regressions on Independent Slopes Model (PRISM) precipitation adjustments (Daly et al. 2008; <http://prism.oregonstate.edu>) and the other meteorological forcing data come from the North American Regional Reanalysis (Mesinger et al. 2006).

Half-hourly and hourly resolution data are averaged into 5-day means. Where data are available to present, we analyze through 2017 because 2018 is not yet complete. We validate the NLDAS-2 LSMs used in this study by comparing their data for the grid points and

TABLE 2. Summary of other datasets.

Dataset	Temporal Availability	Resolution	Variable
NLDAS-2 Noah, Mosaic, VIC	1979–2018	1/8°, hourly	Precipitation, soil moisture, snowmelt evapotranspiration, total runoff
SM-MCDI	1895–2018	1/8°, monthly	Soil moisture 0–200 cm
CLIMGRID	1895–2018	1/24°, monthly	Precipitation, temperature
GIMMS	1981–2015	1/12°, half-monthly	NDVI
NCEP–NCAR Reanalysis	1948–2018	2.5°, monthly	SST, 200-mb geopotential height
USGS gauged streamflow	1979–2018	Monthly	Streamflow (09512500, 09402000, 09504500, 09510000)

time period that correspond to the in situ AmeriFlux sites within the dual season region (where both winter and summer precipitation peaks are observed in the mean annual cycle). In general, sufficient agreement exists between the in situ observations and the LSM simulations to justify use of the latter for larger scale and longer time period analyses.

For a longer-term perspective, we use monthly estimates of 0–200-cm soil moisture based on a Model Calibrated Drought Index (MCDI) developed by Williams et al. (2017). These estimates cover 1895–2018 and are based on a bucket-type moisture-balance model that was tuned by Williams et al. (2017) to have the temporal persistence properties of 0–200-cm monthly soil moisture simulated by the Noah LSM. The MCDI calculations are forced by monthly precipitation and PET. Monthly precipitation and temperature are from the National Oceanic and Atmospheric Administration CLIMGRID dataset (Vose et al. 2014; available online at <https://www.ngdc.noaa.gov/>). The PET calculation also uses vapor pressure from PRISM gridded monthly mean dewpoint data (Daly et al. 2008), and wind and solar radiation data from NLDAS-2 and the version 2 Princeton Global Forcing Dataset (Sheffield et al. 2006; <http://hydrology.princeton.edu/data/pgf/v2/0.5deg/>). The soil moisture estimates based on the MCDI (hereafter SM-MCDI) agree very well with the NLDAS-2 soil moisture in the SWUS and permit us to examine historical soil moisture extending prior to the 1979 start date of NLDAS-2. Also the MCDI is forced by observational climate datasets that are more accurate than reanalysis data used to force the NLDAS-2 LSMs.

To measure vegetation green-up, we use the Global Inventory Modeling and Mapping (GIMMS) satellite normalized difference vegetation index (NDVI), which is available twice monthly from 1981 to 2015 at 1/12° resolution (Tucker et al. 2004). We also use SST and 200-mb (1 mb = 1 hPa) geopotential height from the NCEP–NCAR Reanalysis at monthly time resolution and 2.5° spatial resolution (available online at <https://www.esrl.noaa.gov/>; Kalnay et al. 1996). We also use gauged monthly streamflow discharge from the U.S.

Geological Survey (USGS) for four different sites within the study region (gauge numbers 09512500, 09402000, 09504500, and 09510000; available online at <https://waterdata.usgs.gov/>). These particular gauges are selected based on length and availability of the streamflow record.

3. Results

a. Characterization of precipitation regime in the SWUS

First, we identify the region of the SWUS where the average seasonal cycle of PRISM precipitation had one or more peaks during 1979–2017 (Fig. 1). To identify the region with two peaks, we divide the seasonal cycle into three seasons: fall–winter [October–March (ONDJFM)], spring [April–June (AMJ)], and summer [July–August (JAS)]. Since we are primarily interested in the region with a winter and summer peak, a grid point is said to have two peaks if the mean fall–winter precipitation is greater than the spring precipitation and the summer precipitation is also greater than the spring precipitation. We also check this against maps of precipitation seasonality for North America (online at <http://www.cpc.ncep.noaa.gov/>).

This two-peak region covers most of Arizona and western New Mexico and extends south into Mexico. Next, a box spanning the northern portion of this bimodal region (red outline shown on Fig. 1) that encompasses the available AmeriFlux monitoring stations is chosen to represent this region later in the study.

b. Observations: The seasonal cycles of precipitation, ET, soil moisture, and vegetation

First, we examine available observations from in situ and remotely sensed data for the two-peak region to investigate the characteristics of precipitation, ET, soil moisture, and vegetation. We also examine how the bimodality varies in terms of location within the study region.

We analyze in situ observations from the AmeriFlux network for 15 different monitoring sites from the SWUS that are located in or near the bimodal region

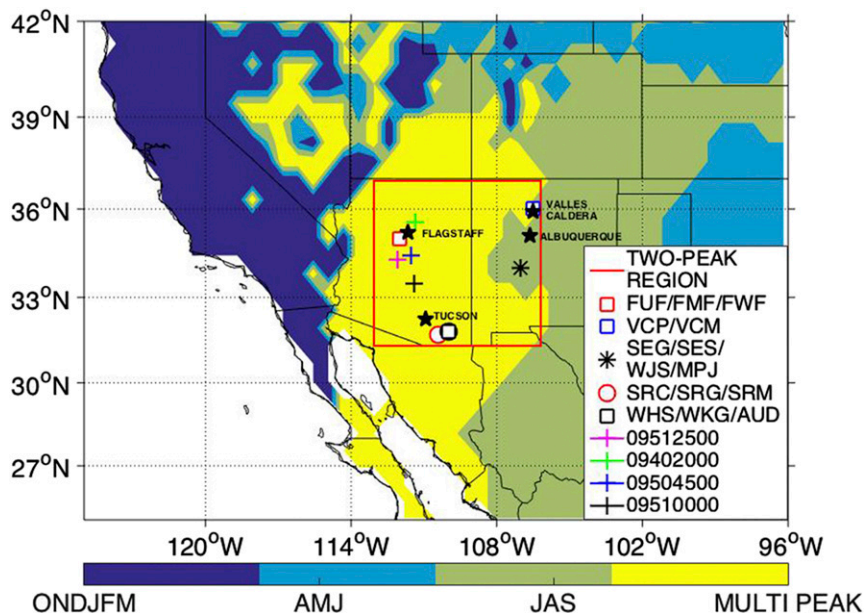


FIG. 1. Map of study area. Shading indicates season of maximum precipitation (ONDJFM, AMJ, JAS, or bimodal). The red box indicates the region used in the study as the bimodal precipitation region. We indicate the locations of the AmeriFlux sites (Fwf, Fuf, Fmf, Vcp, Vcm, Seg, Ses, Mpj, Wjs) and the USGS gauges (09512500, 09402000, 09504500, 09510000).

identified in Fig. 1 (descriptions in Table 1, location shown in Fig. 1). The seasonal cycles of precipitation for each of the 15 sites are shown in Figs. 2a–e and compared with the NLDAS-2 precipitation forcing for the same location and temporal availability (we save a quantitative evaluation between the AmeriFlux and NLDAS-2 simulations for section 3c below). Each of the 15 sites receives precipitation in the winter months, but the seasonal cycle is dominated by the NAM with maximum precipitation occurring during the summer. Each site also has a dry season occurring during the late spring–summer. The seasonal cycle of AmeriFlux ET (Figs. 2f–j) also shows bimodality: a smaller peak in ET during the early spring (March–April), declines to May–June, then increases to a second and greater peak during the summer.

Intersite differences exist in the precipitation and ET among the various AmeriFlux stations. The southern sites (SRC, SRG, SRM, Whs, Wkg, Aud) show a more dominant ET peak during the summer compared to the more northern sites. The highest precipitation during the main NAM season occurs at the Flagstaff, Arizona, sites (Fmf, Fwf, Fuf), presumably because of their higher elevation (2160–2270 m). The next-greatest NAM precipitation peak occurs at the southern sites (Whs, Wkg, Aud) near Tucson, Arizona, closer to the core of the monsoon.

We also examine the seasonal cycle of soil water content (which measures soil water from the top

~10 cm) from the available AmeriFlux sites (Figs. 3d–f). Observations of soil water content indicate two peaks in soil moisture: for the northern sites [Fmf, Fwf, Fuf (Figs. 3a,d)], the largest peak occurs during the late winter to spring (February–March), after which soil moisture declines to a minimum in AMJ, before increasing to a second and smaller peak in the summer monsoon season (JAS). The more southern sites [SRC, SRG, SRM (Figs. 3b,e) and Whs, Wkg, Aud (Figs. 3c,f)] have a peak in winter soil moisture earlier in the year (December–March). The southern sites also have peak in summer soil moisture that is greater in magnitude than the winter peak and occurs in JAS.

Next we examine the seasonal cycle of vegetation in the bimodal region using observations of NEP from the AmeriFlux network (Figs. 4k–o) and GIMMS NDVI (Figs. 4f–j). NEP is defined as the difference between gross primary production and total ecosystem respiration. When the NEP is positive, this indicates vegetation green-up, when negative it indicates vegetation senescence.

NEP peaks twice annually for the different AmeriFlux sites: once in the early spring (March–April), and again in the summer (JAS). The dry season (indicated by vegetation senescence) lies in approximately May–July for the different sites. Intersite differences exist between the AmeriFlux stations due to differences in vegetation type, elevation, and location (details in Table 1). For example, of the Flagstaff sites (Fig. 4l), the managed (Fmf) and

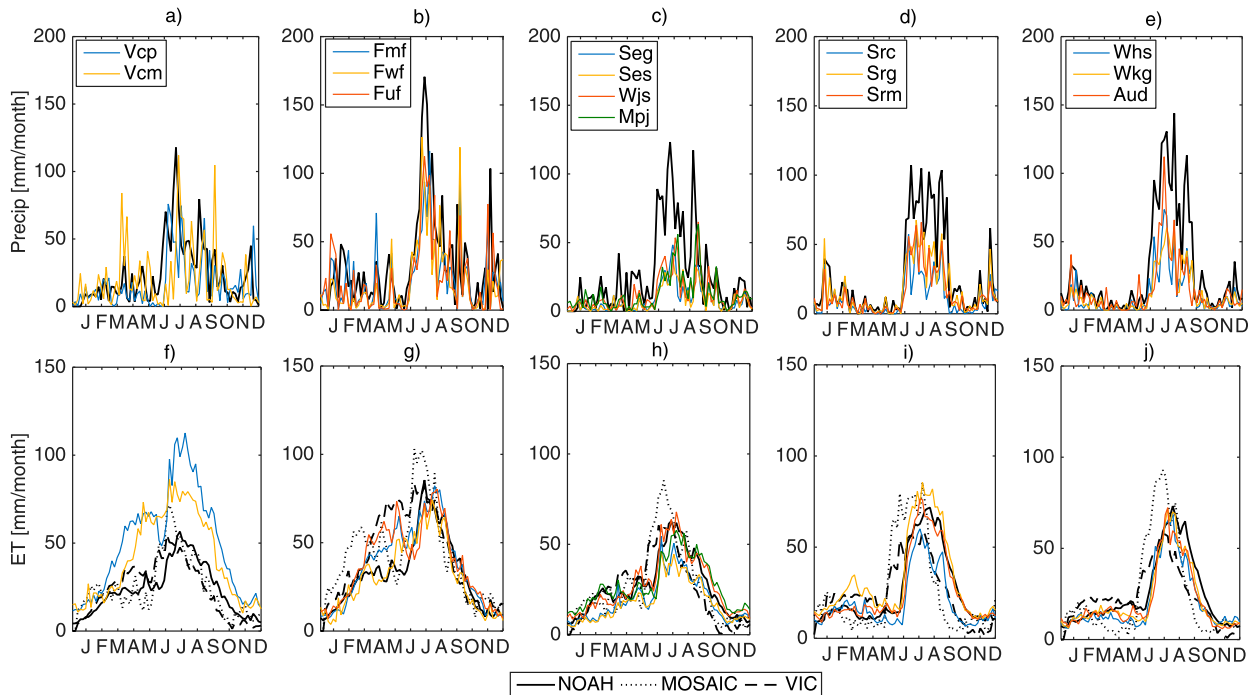


FIG. 2. Comparison of NLDAS-2 and AmeriFlux sites in the bimodal precipitation region for (a)–(e) precipitation (each LSM uses the same precipitation forcing) and (f)–(j) ET. Output from the NLDAS-2 models (Noah, Mosaic, VIC) corresponds to the grid point location of each of the AmeriFlux sites for the corresponding time period available (Vcp, Vcm sites 2007–14; Fmf, Fwf, Fuf sites 2005–10; Seg, Ses, Wjs, Mpj sites 2007–14; SRC, SRG, SRM sites 2008–14; and Whs, Wkg, Aud sites 2007–14). Both NLDAS-2 and AmeriFlux data are plotted at a temporal resolution of 5-day means.

unmanaged (Fuf) evergreen needleleaf forests have larger values of NEP than the other nearby grassland wildfire site (Fwf), as has been noted in previous studies (Dore et al. 2010; Sullivan et al. 2011). The NEP is higher for the Flagstaff (Fig. 4l) and Valles Caldera (Fig. 4k) sites than for the Sevilleta grass and shrubland sites (Fig. 4m), which is expected given the vegetation type (evergreen forest versus open shrublands). The more southern sites [SRC, SRG, SRM (Fig. 4o) and Whs, Wkg, Aud (Fig. 4n)] also have a much larger summer vegetation peak than spring peak consistent with the dominance of summer precipitation (Figs. 2d,e).

The observational GIMMS NDVI is not very consistent with the AmeriFlux pattern of bimodal vegetation greening at each of the sites. For the northern sites the GIMMS NDVI does not show the bimodal greening seen in AmeriFlux NEP, while for the central and southern sites bimodality is muted and the timing seen in NEP is not reproduced.

c. Evaluation of NLDAS-2 LSMs with AmeriFlux and GIMMS NDVI

Next, we assess how well the NLDAS-2 LSMs simulate the climate characteristics (ET, soil moisture, vegetation growth) of the region before using them to

investigate longer term trends. This is necessary due to the localized nature and short time period of the AmeriFlux site data.

In Figs. 2 and 5 the seasonal cycles of precipitation, ET, soil moisture, and NEP of the AmeriFlux sites in the bimodal region of the SWUS are compared with NLDAS-2 LSM simulations, and, in general, there is good agreement. The largest differences in precipitation for the two datasets occur at the central-eastern and southern Arizona sites where monsoon precipitation is too high in NLDAS-2. Using Pearson's correlation we find the r values between the seasonal cycle of precipitation from NLDAS-2 forcing and AmeriFlux sites varies from a low value of $r = 0.37$ of the northern Valles Caldera site (Vcm) to $r = 0.93$ at the Tucson site (Wkg).

NLDAS-2 LSMs and AmeriFlux measurements are also in general agreement ($r > 0.5$) on the mean annual cycle of ET (Table 3). The largest difference between AmeriFlux and NLDAS-2 ET occurs at the Valles Caldera northeastern site where NLDAS-2 ET is half that in AmeriFlux. For the other 13 sites the magnitude and seasonal cycle of ET agree reasonably well between AmeriFlux and NLDAS-2. The r values for ET from the AmeriFlux sites are greater with NLDAS-2 Noah than with either Mosaic or VIC.

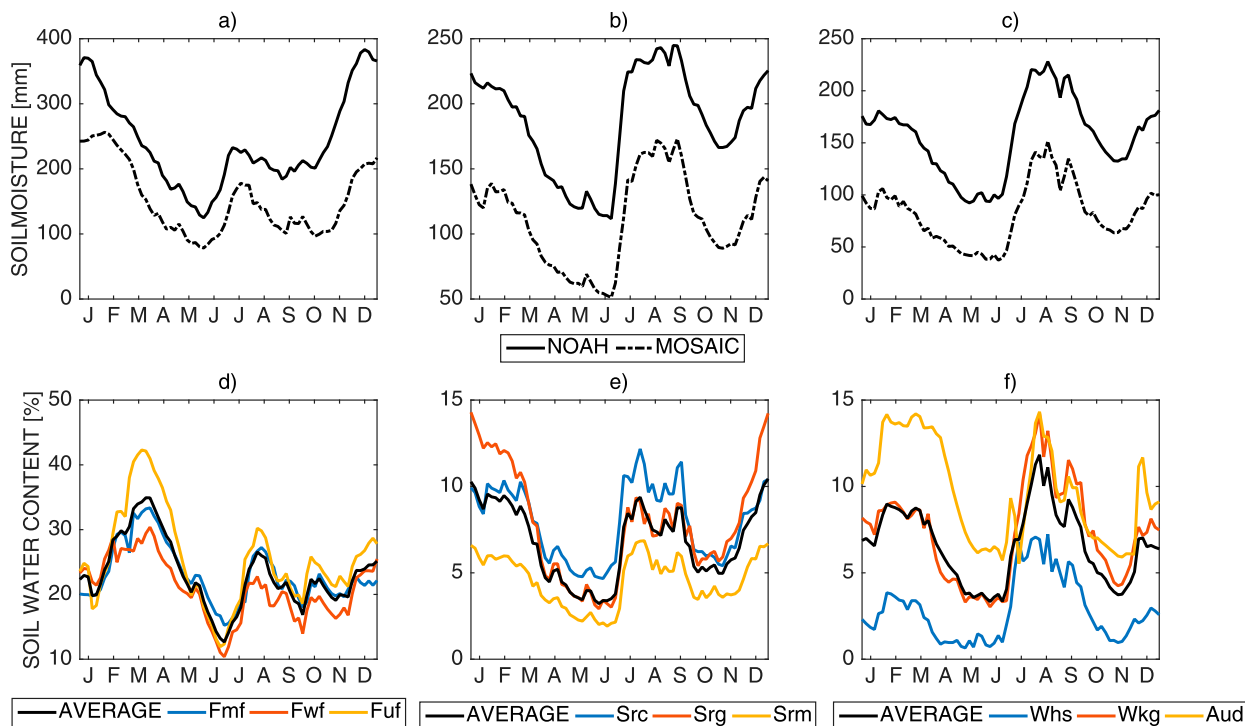


FIG. 3. Seasonal cycle of NLDAS-2 (Noah, Mosaic) (a)–(c) 0–10-cm soil moisture compared with AmeriFlux (d)–(f) soil water content (%; derived from upper 10 cm of soil moisture). This level is the only one available from the AmeriFlux network, which is why we use it to compare with NLDAS-2. The NLDAS-2 soil moisture corresponds to the grid point location and available time period of the AmeriFlux site used (Fmf, Fwf, Fuf; SRC, SRG, SRM sites; and Whs, Wkg, Aud sites). Both NLDAS-2 and AmeriFlux data are plotted at a temporal resolution of 5-day means.

Turning to soil moisture (0–10 cm), NLDAS-2 Noah and Mosaic (0–10 cm is not reported by VIC) are characterized by a bimodal seasonal cycle for the Flagstaff sites, but the winter peak is earlier in the year (January–February) compared to the AmeriFlux observations (March) (Figs. 3a,d). Away from the Flagstaff sites, LSM soil moisture broadly agrees with the observed soil water content. The other more southern AmeriFlux sites have earlier winter soil water content peaks (January–February) and these compare well in timing with the NLDAS-2 soil moisture which also peaks at this time (correlation coefficients between the AmeriFlux sites and NLDAS-2 models are shown in Table 3). The summer maximum occurs in June–September, and also agrees with the simulated NLDAS-2 soil moisture. The timing of the spring dry season is comparable across the region, and occurs in AMJ. The timing of the soil moisture increase that ends the spring dry season also agrees between the AmeriFlux sites and NLDAS-2, except for the Flagstaff sites where NLDAS-2 is one month too early. We speculate that the earlier soil moisture peak could be due to snowmelt in this region occurring too early in the NLDAS-2 models.

We compare observations of NEP and NDVI with NLDAS-2 prescribed LAI (Fig. 4) and present correlation

coefficients between the models and observations (Tables 4 and 5). We find that AmeriFlux NEP correlates best with Noah LAI (Table 4, top row). Mosaic and VIC LAI for the most part have correlations which are not significant at $\alpha = 0.05$. Turning to correlations with GIMMS NDVI and NLDAS-2 LAI, we find that Mosaic agrees the most with the satellite NDVI (Table 5). We caveat this analysis with the fact that NEP, NDVI, and LAI are not the same quantity and not directly comparable. However, we find that in general NLDAS-2 LAIs (in particular Noah and Mosaic) simulate vegetation bimodality in this region.

Based on these results, we find that overall the Noah model best represents the observations, and we therefore use it in subsequent analyses.

d. Relationship of vegetation green-up with soil moisture

Previous studies have indicated the importance of soil moisture to vegetation green-up (Notaro et al. 2010; Muldavin et al. 2008; Huxman et al. 2004; Scott et al. 2009; Vivoni et al. 2008; Watts et al. 2007), and therefore soil moisture can be considered as an indicator of ecosystem productivity. We explore this relationship using

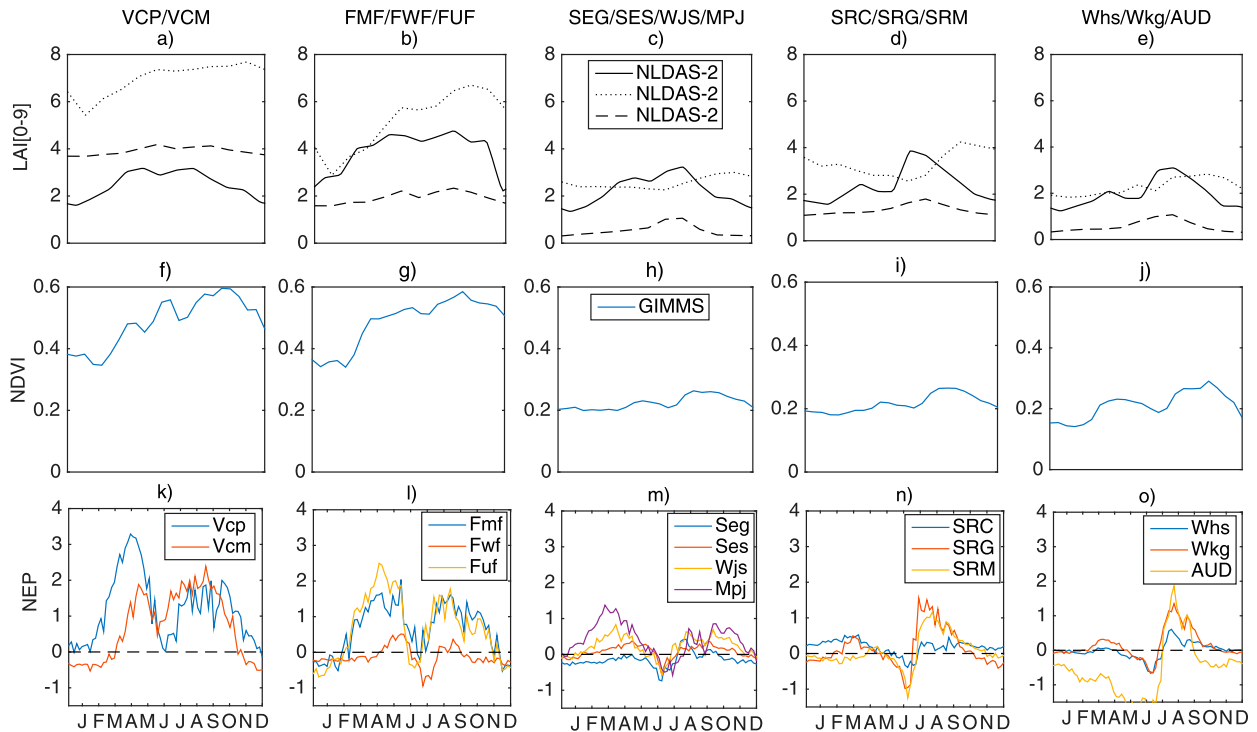


FIG. 4. (a)–(e) Seasonal cycle of NLDAS-2 Noah, Mosaic, and VIC LAI (0–9), (f)–(j) GIMMS NDVI, and the (k)–(o) negative of AmeriFlux net ecosystem exchange. Net ecosystem exchange (NEE) is defined as the total respiration (autotrophic plus heterotrophic) minus net primary production (NPP) and reflects ecosystem exchange of carbon with the atmosphere. During the growing season when productivity exceeds respiration, NEE is negative. Here we plot the negative of NEE (NEP) in order to better visualize plant growth. The NLDAS-2 LAI and GIMMS NDVI corresponds to the grid point location and available time period of the AmeriFlux site used.

the AmeriFlux NEP and NLDAS-2 Noah soil moisture within the two-peak region.

Time series of vegetation green-up and soil moisture are shown in Fig. 5. We create composites across sites and years of NEP from the 15 AmeriFlux sites over the period of overlap (2007–10) in 5-day means for the more northern and east-central sites (Fig. 5, top panel) and southern sites (Fig. 5, bottom panel). This is compared with a composite of Noah soil moisture (0–10 cm) at the grid point locations of the AmeriFlux sites. We choose to use the model soil moisture since it provides a more continuous record of soil moisture than the AmeriFlux data (which has missing data in the time series). As a caveat we note that NLDAS-2 Noah vegetation is prescribed and has the same seasonal cycle each year, which will in turn influence soil moisture draw down. Therefore, we expect soil moisture to not completely track the observations of NEP from AmeriFlux.

The peak in winter soil moisture occurs during the low vegetation productivity winter months. NEP then increases during spring and draws down the soil moisture. This is more prominent among the northern sites (top panel). The NEP then declines when soil moisture has been drawn down to low values prior to the summer

monsoon. The second maximum of NEP then follows after the monsoon driven summer maximum in soil moisture. An exception occurs in 2009 in which NAM rainfall was significantly below average (verified in records of PRISM precipitation for the summer of 2009). The green-up of vegetation with the NAM is particularly striking for the southern sites, which have greater vegetation productivity during summer and only a muted spring green-up despite a clear spring soil moisture maximum. This is consistent with the southern sites being dominated by C4 grasses which are more sensitive to summer conditions (Notaro et al. 2010).

For 2007–10 at the northern and southern sites, we also examine the seasonal evolution of NEP with soil moisture and precipitation. We create individual scatterplots (see Fig. A1 in the appendix) of NEP against soil moisture, and join the points to illustrate the evolution of each quantity in time, and also in terms of precipitation (indicated by shading of line). We find that for the northern sites (Fig. A1, top panel) the average path taken is as follows: soil moisture begins high in the winter months with winter precipitation, while NEP is low (January–February). NEP then increases as soil moisture is drawn down in the early spring (March–May). After this initial

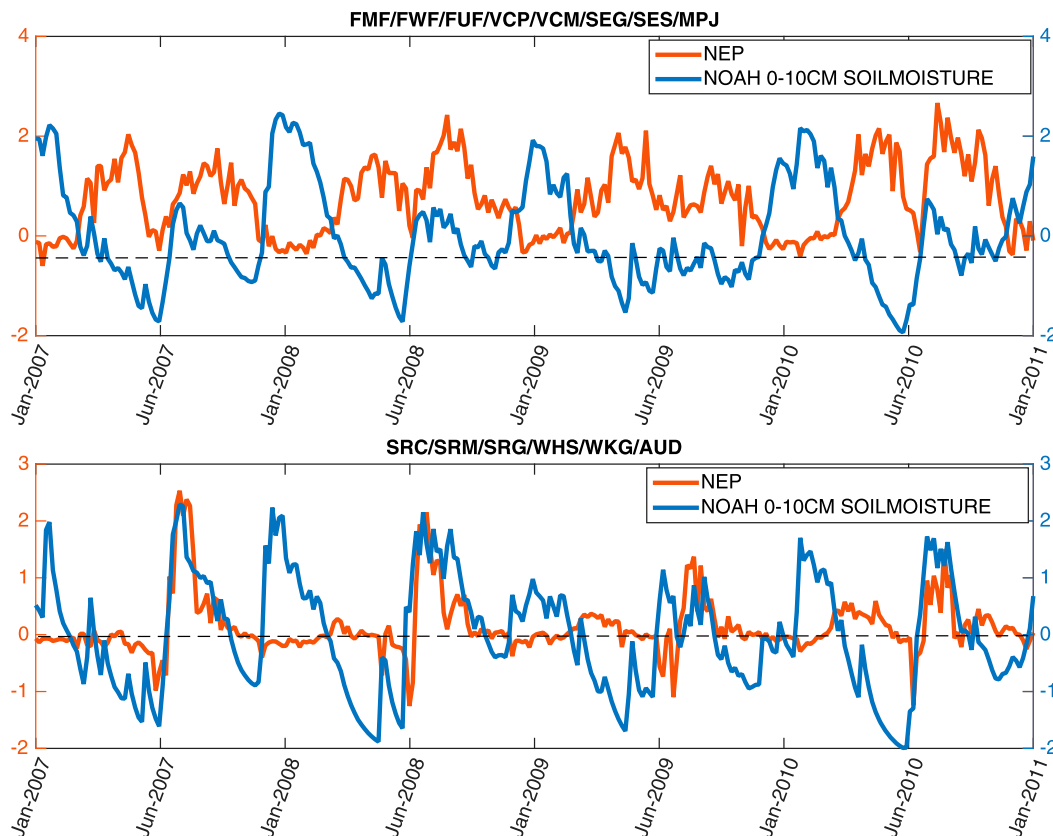


FIG. 5. Composite of NEP for AmeriFlux sites (red line) and standardized Noah 0–10-cm soil moisture corresponding to sites (blue line). Data are in 5-day means for 2007–10. (top) Northern sites (Fmf, Fwf, Fuf, Vcp, Vcm, Seg, Ses, Srm, Mpj) and (bottom) southern sites (SRC, SRG, SRM, Whs, Wkg, Aud).

spring green-up, precipitation is low, and NEP then begins to decline (this is the spring dry season from May to June). Soil moisture and NEP then both increase with a pulse in precipitation during the summer monsoon months (July–September). The scatterplot for the southern sites (Fig. A1, bottom panel) also demonstrates the decline in soil moisture and NEP from the winter into the spring, and then the increase in either quantity following the arrival of the monsoon (July–September).

Analysis of the observations indicate a coupled relation between NEP and soil moisture [consistent with previous studies (Notaro et al. 2010; Muldavin et al. 2008;

Huxman et al. 2004; Scott et al. 2009; Vivoni et al. 2008; Watts et al. 2007)]. Hence, we use soil moisture as an indicator of the dry season due to its association with ecosystem productivity and its long period of record.

e. Larger SWUS bimodal region: Seasonal cycle of precipitation, ET, and soil in NLDAS-2 Noah

Next, we turn our analysis to the broader SWUS bimodal area identified in Fig. 1. We use spatially averaged precipitation, ET, and soil moisture (0–200 cm) to create seasonal cycles in 5-day means from 1979 to 2017 from the Noah output (Fig. 6). First, we correlate the

TABLE 3. Correlation of NLDAS-2 LSM output with AmeriFlux (r values significant at $\alpha = 0.05$ unless surrounded by parentheses).

	Vcp	Vcm	Fmf	Fwf	Fuf	Seg	Ses	Wjs	Mpj	SRC	SRG	SRM	Whs	Wkg	Aud
Precipitation	0.48	0.37	0.57	0.58	0.61	0.68	0.65	0.62	0.57	0.76	0.85	0.86	0.92	0.93	0.82
ET (Noah)	0.96	0.91	0.92	0.93	0.85	0.92	0.94	0.97	0.93	0.92	0.97	0.98	0.95	0.97	0.96
ET (Mosaic)	0.71	(0.21)	0.73	0.78	0.66	0.79	0.79	0.58	0.65	0.57	0.54	0.56	0.81	0.75	0.76
ET (VIC)	0.83	0.28	0.89	0.86	0.88	0.77	0.76	0.48	0.64	0.72	0.75	0.72	0.79	0.78	0.80
0–10-cm SM (Noah)	—	—	(-0.05)	0.36	(0.13)	—	—	—	—	0.88	0.74	0.90	0.87	0.95	0.46
0–10-cm SM (Mosaic)	—	—	(0.11)	0.51	(0.23)	—	—	—	—	0.89	0.69	0.89	0.86	0.94	0.48

TABLE 4. Correlation of NLDAS-2 LSM LAI with AmeriFlux NEP (r values significant at $\alpha = 0.05$ unless surrounded by parentheses).

	Vep	Vcm	Fmf	Fwf	Fuf	Seg	Ses	Wjs	Mpj	SRC	SRG	SRM	Whs	Wkg	Aud
LAI (Noah)	0.61 (0.22)	0.85 (0.66)	0.80 (0.52)	0.36 (0.14)	0.67 (0.35)	0.29 (0.38)	0.26 (0.26)	0.14 (0.46)	(-0.2)	-0.30 (0.44)	0.67 (0.05)	0.54 (0.32)	0.34 (0.49)	0.65 (0.52)	0.49 (0.54)
LAI (Mosaic)	(0.34)	0.87	0.78	(0.28)	0.64	(-0.24)	(-0.32)	(-0.44)	(-0.6)	(-0.04)	(-0.15)	(-0.25)	(-0.29)	(0.17)	(0.06)

seasonal cycle of 5-day mean precipitation and ET from the average of the 15 AmeriFlux sites and the corresponding NLDAS-2 grid points, and find that over the greater region, precipitation agrees at $r = 0.79$ and ET at $r = 0.91$. These high correlation values for the broader area give us confidence in using the spatially averaged Noah simulations for the rest of the analysis.

The 0–200-cm soil moisture shows a maximum in winter followed by a drying in the spring, which is restored to a smaller secondary peak in the summer. The 0–200-cm soil moisture has the same bimodal pattern as the 0–10-cm values, but, the winter and summer peaks occur later in the year and are more muted. The larger winter peak arises due to both the steady nature of precipitation in the winter months, allowing water to readily infiltrate the soil, and cooler temperatures and low evaporative demand (Loik et al. 2004). In the summer, monsoon precipitation is overall greater in magnitude and more intense, but also is short lived occurring in convective storms, and much of this water is lost to surface runoff. This is an increasingly important mechanism farther south in the study region where monsoon precipitation dominates and the surface runoff to precipitation ratio is large (not shown). In addition, evaporative demand is also much greater during the summer, leading to soil moisture drawdown.

f. Decadal shifts

We examine two periods over the last three decades to contrast changes in the dry season and vegetation green-up in the bimodal region: 1979–97 and 1999–2017. These periods are selected based on the climate shifts observed over the tropical Pacific which are known to have implications for the SWUS (Zhang et al. 1997; Mantua et al. 1997). We also ensure both periods are of equal length (19 years), and select 1979–97 to capture the particularly wet year 1979. The recent dry period is chosen to start in 1999 as this excludes the wet year 1998 (resulting from the 1997/98 El Niño), and captures the more severe dry years of the recent period. We end the period in 2017 to ensure complete years of data, but note that this drought is ongoing in 2018.

However, since GIMMS NDVI begins in 1981, it is averaged over the bimodal region for 1981–97 and 1999–2015 (Fig. 7). NDVI is significantly lower during March–July in the later decades: using a Student's t test significant at $\alpha = 0.05$, we compared the distribution of NDVI values in each period and found the distributions to have different means for all months from March to July. There is no significant decline in the later summer months in NDVI. A slight shift to later start in green-up is also observed in later decades for the mean seasonal cycle, with green-up starting in mid-February for 1999–2015

TABLE 5. Correlation of NLDAS-2 LSM LAI with GIMMS NDVI (r values significant at $\alpha = 0.05$ unless surrounded by parentheses).

	GIMMS (Vcp, Vcm)	GIMMS (Fmf, Fwf, Fuf)	GIMMS (Seg, Ses, Wjs, Mpj)	GIMMS (SRC, SRG, SRM)	GIMMS (Whs, Wkg, Aud)
LAI (Noah)	0.45	0.67	0.22	0.48	0.43
LAI (Mosaic)	0.89	0.94	0.70	(0.56)	0.81
LAI (VIC)	0.60	0.73	(-0.08)	(0.35)	(0.1)

compared to early February (1981–97) (Fig. 7). However, this delayed green-up start is found not to be significant when we test the distribution of green-up start times in either period (using a Student’s t test we find $t = 1.06$, $p = 0.29$).

Seasonal cycles of rain, snowfall, total runoff, snowmelt, soil moisture (0–200 cm), ET, the ratio of snow to total precipitation, and SWE from NLDAS-2 Noah are shown in Fig. 8. The seasonal cycles are averaged over the same two time periods: 1979–97 and 1999–2017. A drying is observed in each of these quantities for the later decades. Rain is reduced in the winter–spring (Fig. 8a), but no significant change occurs during the summer monsoon season. SWE and snowmelt are also reduced in the later decades (Figs. 8d,h). Soil moisture also declines and shifts to an earlier spring minimum in the later decades (Fig. 8e). The mean minimum occurs on average one week earlier in the later decades, but this earlier timing is not significant when testing the timing for the distribution of years from either period (using a Student’s t test we find $t = 0.29$, $p = 0.78$). Runoff is also reduced, particularly during the winter runoff peak (Fig. 8c). To verify the shift toward reduced runoff, as well as the magnitude of this reduction, we examine the same decadal seasonal cycles of USGS gauged streamflow data for a number of sites within the region, and find the same marked decline between either time period (see Fig. A2 below).

To place these changes in the SWUS region in the context of planetary scale Pacific decadal variability, the continent-wide spatial patterns of the difference between the two periods are shown in Fig. 9 for annual average precipitation, ET, total runoff, snowmelt, soil moisture (0–200 cm), air temperature, along with Pacific–North America patterns of detrended SST and 200-mb geopotential height. Drying in the later decades is apparent across the SWUS for each of the hydrological variables, as well as a widespread increase in temperature across much of the continental United States. This pattern of drying during the later decades is consistent with the tropical Pacific influence on winter precipitation in the SWUS (Delworth et al. 2015; Seager and Vecchi 2010; Mantua et al. 1997; Huang et al. 2005). After the 1997/98 El Niño, there was a shift to cooler SST and low geopotential heights over the tropical

Pacific and positive 200-mb geopotential height anomalies over the west which cause the drying (Delworth et al. 2015; Seager and Vecchi 2010; Lehner et al. 2018). The same patterns associated with the Pacific are apparent for the midcentury drought (see Fig. A3 below).

We create a metric of spring drying based on soil moisture from Noah and SM-MCDI (Fig. 10, top panel). We define the length of the dry season as the period of drying between the winter maximum in soil moisture and the spring minimum, before recovery with summer precipitation. We use the deeper depth (0–200 cm) soil moisture for Noah to be consistent with the SM-MCDI. No significant trend in the duration of the dry season is detected during 1979–2017 (based on results of a Mann Kendall significance test we find $\tau = 8.22$, $p = 0.30$ and $\tau = -75.79$, $p = 0.83$ for Noah and SM-MCDI, respectively).

For the soil moisture minimum, for 1979–97 the average minimum occurs during the second week of July, and for 1999–2017 the minimum occurs in the first week

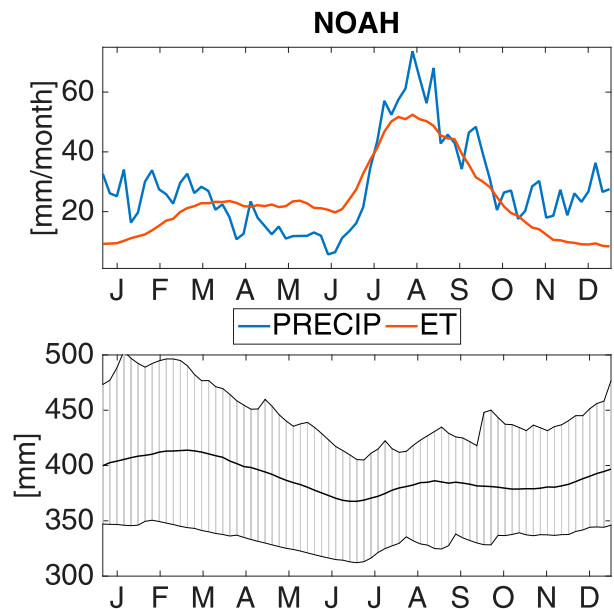


FIG. 6. Seasonal cycle of the bimodal region for (top) precipitation and ET and (bottom) soil moisture (0–200 cm) for NLDAS-2 Noah time averaged from 1979 to 2017. Shading on soil moisture indicates the variability over the years averaged.

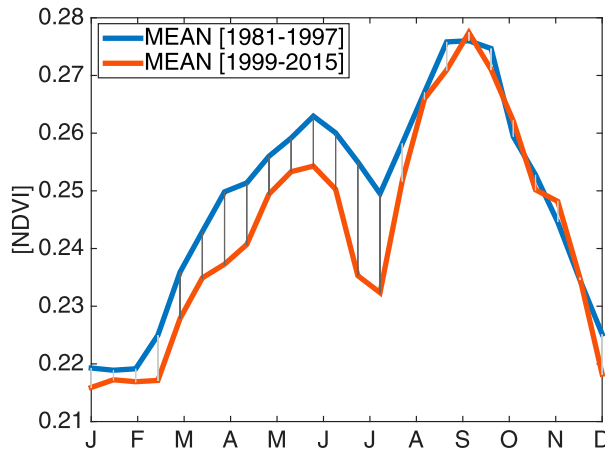


FIG. 7. Seasonal cycle of GIMMS NDVI area averaged over the bimodal precipitation region (indicated in Fig. 1). The seasonal cycles for two different decadal periods are shown: 1981–97 and 1999–2015. Vertical solid black lines indicate the difference is significant (using a Student's t test at a 0.05 significance level to each half-month distribution from the different periods), and gray lines indicate the difference is not significant between the two periods.

of July (Fig. 10b). This shift toward an earlier spring minimum is found to be significant for the average of Noah and SM-MCDI (based on results of a Mann Kendall significance test with $\tau = -3.50$, $p = 0.01$). However, individually, only SM-MCDI has a significant trend toward an earlier spring soil moisture minimum.

Examining the average trend for the winter soil moisture peak in Noah and SM-MCDI, we find that from 1979 to 1997, the average peak is the third week of February, and for 1999–2017, the first week of February (Fig. 10c). However this trend toward an earlier peak is not significant (based on results of a Mann Kendall significance test with $\tau = -6.53$, $p = 0.19$).

The earlier spring minimum is consistent with less total moisture being delivered to soils in the winter and spring, and hence the same drying rate achieves the soil moisture minimum earlier in the season. The lack of trend in the duration of the dry season is consistent with both the winter peak and spring minimum shifting to earlier in the year.

g. Simple soil moisture balance model

To better understand the processes responsible for the decadal differences in soil moisture we relate the change in soil moisture dS_m/dT to rain P_{rain} , snowmelt S_n , ET, and runoff R_o using the following

$$\frac{dS_m}{dt} = \frac{S_{m_t+\Delta t} - S_{m_t}}{\Delta t} = P_{\text{rain}} + S_n - \text{ET} - R_o. \quad (1)$$

We use the seasonal cycles of P_{rain} , S_n (both defined positive as a soil moisture gain), ET, and R_o (both

defined positive as a soil moisture loss) in the bimodal SWUS region from NLDAS-2 Noah output to calculate dS_m/dT at each 5-day time step using values from the wet decades (1979–97) and the dry decades (1999–2017) (Fig. 11a). We calculate dS_m/dT by integrating forward in time using values of P_{rain} , S_n , ET, and R_o at a time step Δt of one pentad.

The results of the soil moisture balance model are compared with Noah 0–200-cm soil moisture for each of these two decades. We use this deeper depth as it produces the best agreement with the output from our simple model, and is also consistent with the depth of the SM-MCDI soil moisture that we analyze later. Like the 0–100-cm soil moisture layer, the 0–200-cm layer has more muted and later winter and summer peaks than the 0–10-cm layer, but still has a clear connection with vegetation green-up and decay in the spring and summer. The calculated soil moisture from the simple model generally agrees with the output from NLDAS-2 Noah in either decadal period.

We then decompose the change in soil moisture balance into contributions from P_{rain} (Fig. 11b), S_n (Fig. 11c), ET (Fig. 11d), and R_o (Fig. 11e). Rain and snowmelt from the later decades drive the observed soil moisture decline, with rain producing the greatest change. This is consistent with the study region being mostly dominated by rain with just a subset of the northern sites having snow cover during the winter. Rain also produces the observed shift to an earlier spring dry period. From the point of view of soil moisture, reductions in runoff and ET are then offsetting responses arising from the reduced soil moisture availability.

h. Contrasting the 1948–66 and 1999–2017 droughts

The decadal shift to drier conditions in recent decades need not be due to long-term climate change. Decadal variability is strong in this region of the SWUS, as evidenced in the SM-MCDI soil moisture extending back to 1948 (Fig. 12). We focus on 1948 to present due to the greater accuracy of climate data and availability of comprehensive atmospheric reanalysis in the second half of the twentieth century. For the midcentury drought, we select the years 1948–66 so that we are capturing the driest years during the midcentury period, and also so that we are contrasting two time periods of equal length (19 years).

The 1950s drought is prominent in the historical time series, with soil moisture values falling almost as low as the current period of drying (1999–2017). This drought in the SWUS is well documented, and is associated with tropical Pacific SST anomalies and a ridge over the SWUS (also see Fig. A3) (Seager et al. 2005; Cook et al. 2011). It appears amid an extended midcentury dry

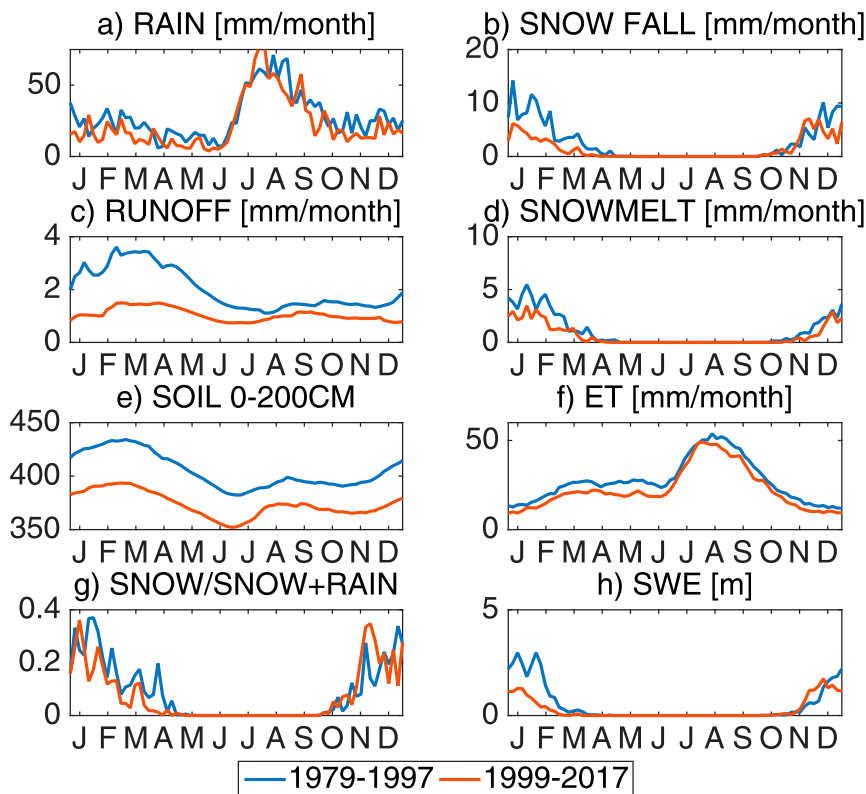


FIG. 8. NLDAS-2 Noah seasonal cycle of the bimodal region showing the decadal shift of hydrological variables for wet decades (1979–97) and dry decades (1999–2017) for (a) rain, (b) snowfall, (c) total runoff, (d) snowmelt, (e) soil moisture (0–200 cm), (f) ET, (g) the ratio of snow to total precipitation, and (h) SWE.

period that continued until the late 1970s and was also related to cool tropical Pacific SSTs (Huang et al. 2005).

Based on the SM-MCDI soil moisture, we find that soil moisture was lower in the more recent drought throughout the year compared to the 1940s/50s drought (Fig. 13b). This is hard to explain in terms of a precipitation decrease given the small difference between precipitation in the midcentury and recent drought (Fig. 13a). The lack of explanatory power from precipitation change has also been noted in a study contrasting droughts in the upper Colorado River basin during the twentieth century (Woodhouse et al. 2016). The temperature anomalies show more striking decadal changes, with the most recent drought having greater temperatures in each month of the year, compared to both the previous drought and the 1979–97 wet period (Fig. 13c).

In light of warming temperatures in the region, we use the SM-MCDI soil moisture to investigate specifically the role of evaporative demand in each drought. In Fig. 14 the spring (AMJ) SM-MCDI soil moisture is plotted as an anomaly relative to the 1921–2000 mean (bars) and is then decomposed to show the contribution

of precipitation (SM-P, blue line) and PET (SM-PET, red line). SM-P is forced by precipitation only, holding PET at its mean annual cycle for 1921–2000. The difference between SM-MCDI and SM-P (SM-MCDI minus SM-P) is the effect of PET on soil moisture (SM-PET) (Williams et al. 2017). For the midcentury drought (1948–66) PET contributed to 6% of the negative soil moisture anomaly, and for the recent drought (1999–2017), PET contributed to 39% of the soil moisture anomaly.

This analysis confirms the results of other studies (Woodhouse et al. 2016), indicating the heightened role of temperature in exacerbating drying during the more recent drought despite similar precipitation amounts. This finding is consistent with the shift to warmer temperatures in the region throughout the year (Fig. 13). As such, warming and higher evaporative demand lead to lower soil moisture in the spring in the most recent drought than in the prior drought, despite similar reductions in precipitation. Although not novel, this result demonstrates the sensitivity of hydroclimate in this region to increasing temperatures, with potential implications to future warming. Focusing on the spring period

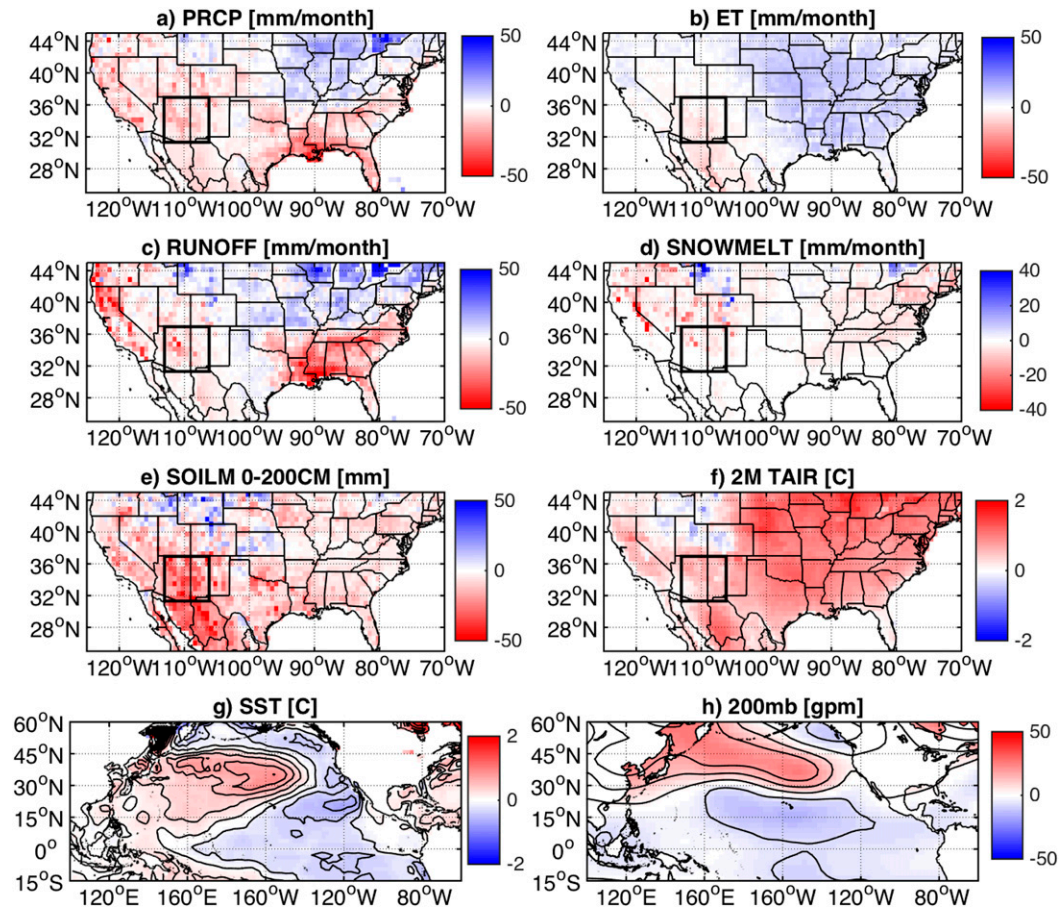


FIG. 9. Maps showing difference in annual average for hydrological variables between dry decades (1999–2017) minus wet decades (1979–97) for (a) NLDAS-2 precipitation forcing, (b) Noah ET, (c) Noah total runoff, (d) Noah snowmelt, (e) Noah 0–200-cm soil moisture, (f) NLDAS-2 temperature forcing (2-m level). For large-scale dynamical context, NCEP–NCAR Reanalysis detrended (g) SST and (h) 200-mb geopotential height are shown. Contours are plotted at 0.25°C intervals for SST, and at 20-m intervals for geopotential height.

is also critical, as the spring is already naturally characterized by limited moisture and vegetation senescence. Our study therefore highlights the importance of temperature in this already moisture-limited season, with implications on runoff, vegetation, and other systems (discussed below).

4. Conclusions

a. How has hydroclimate changed on decadal time scales, and how has this influenced the spring and summer vegetation green-ups?

From 1999 to 2017, precipitation during the winter–spring declined, compared to an earlier wet period (1979–97). This climatic shift in the SWUS is well known, and associated with the change from warmer to cooler SSTs in the tropical Pacific (McCabe et al. 2004; Mantua et al. 1997; Huang et al. 2005). The magnitude

and timing of the NAM was relatively unchanged during this shift.

This climatic shift led to a significant decline in spring vegetation productivity in this region since 1999, according to GIMMS NDVI data, and consistent with previous studies (Notaro et al. 2010; Muldavin et al. 2008; Williams et al. 2013). This is associated with the reduction in winter–spring precipitation, which is critical for adding moisture to soils, and providing water for spring vegetation green-up. Summer vegetation green-up has been relatively unchanged in 1999–2015 compared to 1981–97, and this is due to the lack of change in the NAM during this period. Our results therefore agree with previous studies, and demonstrate that on longer time scales, decadal periods of reduced winter–spring precipitation leads to declines in spring vegetation productivity, but does not impact summer vegetation greening.

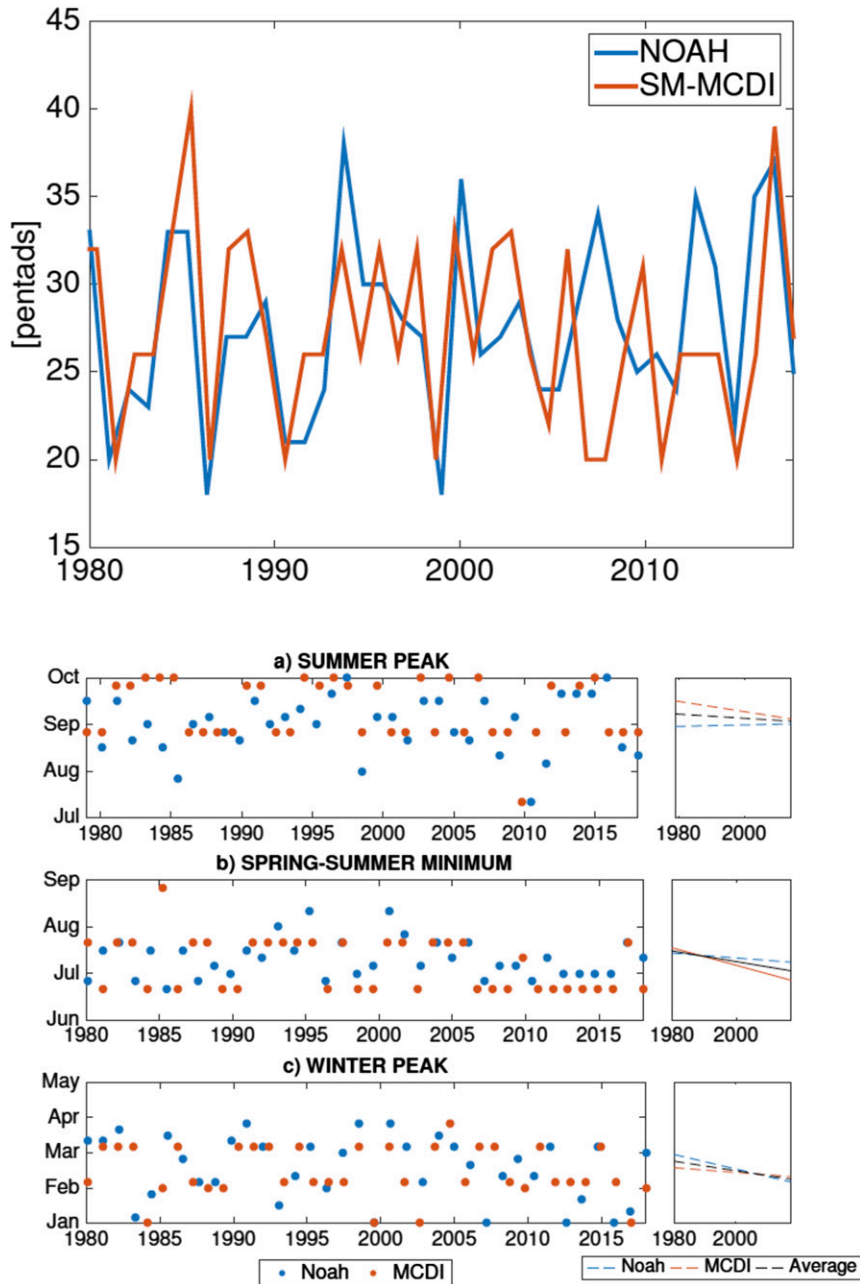


FIG. 10. (top) Time series of the duration in the spring drying period for NLDAS-2 Noah (0–200 cm) and SM-MCDI (0–200 cm). The spring dry season duration is defined as the time between soil moisture winter peak to spring–summer minimum and is plotted in 5-day means (pentads). (bottom) The timing of the (a) summer soil moisture peak, (b) spring–summer minimum, and (c) winter peak in the left panels, with the linear trend shown in the right panels. We use the deeper available soil moisture levels from the models, as these exhibit less year-to-year variability and provide more consistent results in timing across models. Solid (dashed) lines indicate that trends are significant (insignificant) (using a Mann–Kendall significance test at $\alpha = 0.05$).

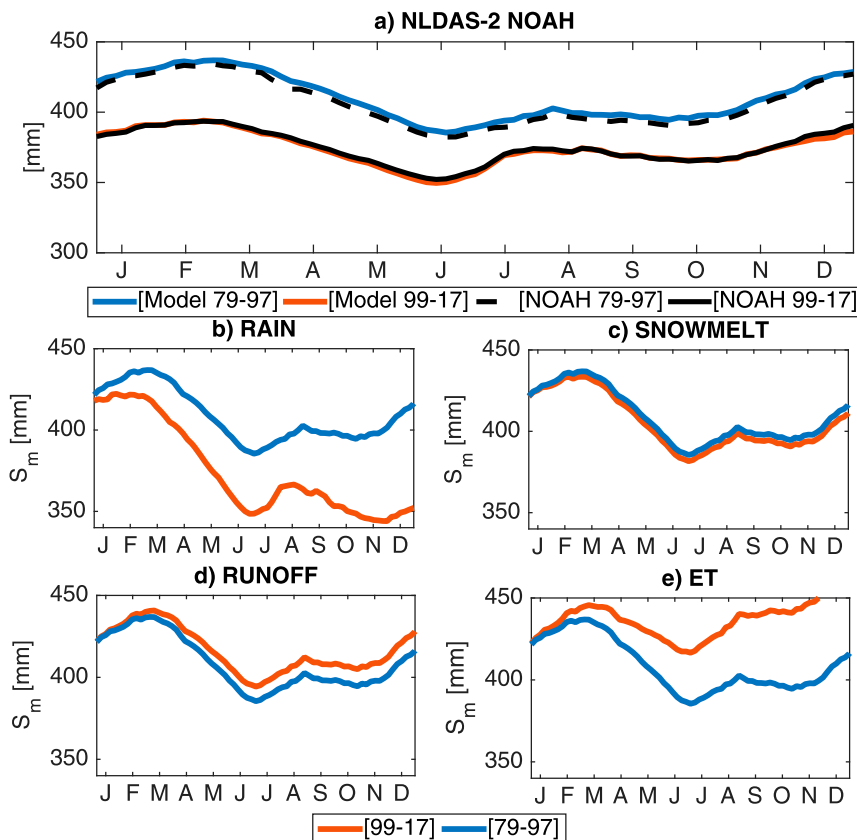


FIG. 11. (a) Simple model for soil moisture (0–200 cm) in the bimodal region run for the wet decades (1979–97) (blue line) and dry decades (1999–2017) (red line). The simple model calculates soil moisture from the balance of rain, snowmelt, ET, and runoff. The simple model is compared with NLDAS-2 Noah soil moisture for either period. Contribution of each variable from the simple model to the observed drying from earlier to later decades. The model is run using the dry decades (1999–2017) value of one variable at a time for each of (b) rain, (c) snowmelt, (d) ET, and (e) runoff] and wet decades (1979–97) values for other variables. This is compared with the modeled wet decades soil moisture.

b. How do shifts in hydroclimate influence the magnitude, timing, and duration of the intervening spring dry season?

From 1999 to 2017, the spring dry season has become significantly drier and has shifted to earlier in the year compared to a prior wet period (1979–97), as represented in the NLDAS-2 Noah model and SM-MCDI soil moisture. There is also a tendency toward earlier winter soil moisture maximum (however, this is found to not be statistically significant). The combined result is to shift the dry season to earlier in the year. The earlier spring minimum is associated with less available moisture in the soils, and therefore the same rates of drying will lead to the minimum being reached earlier in the season. This reduction in moisture availability and faster drying is also reflected in the reduction of spring vegetation green-up in NDVI during this time period.

The lower magnitude and earlier average spring soil moisture minimum are attributed to reduced winter–spring precipitation, more precipitation falling as rain rather than snow during the winter, and earlier snowmelt. Earlier snowmelt in the west has also been well established in the literature (Barnett et al. 2008; Mote et al. 2018). The impact of earlier melt is more important in the northern portion of the study region, which receives greater amounts of snow cover at elevation during the winter months. The dominant mechanism arises from the overall decrease in winter–spring precipitation, which contributes to drying out of the soil moisture column earlier in the year as less moisture is initially available. Implications of this also include a reduction in runoff and NEP, which respond to the magnitude of moisture in the system.

Analysis of twentieth-century soil moisture (SM-MCDI), in conjunction with known periods of drought

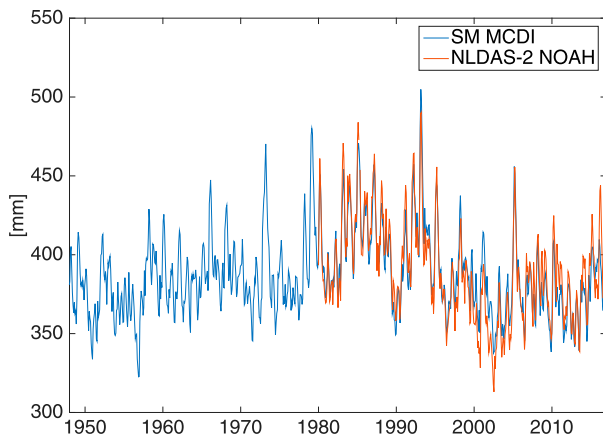


FIG. 12. Time series of 0–200-cm soil moisture for NLDAS-2 Noah (monthly) and SM-MCDI soil moisture (monthly) (Williams et al. 2017).

and pluvials in the mid twentieth-century (Seager et al. 2005; Cook et al. 2011), indicate that this decadal variability in spring drying has been prevalent throughout the past century in the SWUS. We also find that spring drying during the midcentury is associated with the same climate mechanism as for the recent period, and is primarily due to a reduction in winter–spring precipitation.

c. Is there an influence of warming temperatures on the ecohydrology of the region?

In agreement with previous studies (Woodhouse et al. 2016), temperature increases and greater PET during the more recent period were found to enhance drying and soil moisture decline compared to the midcentury drought. The role of PET in soil moisture drying increased from 6% for 1948–66 to 39% in 1999–2017. This suggests that continued rising temperatures will exacerbate soil moisture drying and stresses the sensitivity of this region to anthropogenic warming.

Despite the temperature influence, precipitation plays the dominant role in spring drying for both the midcentury and recent drought as stated above. During the earlier period (1979–97), 25% of precipitation fell as snow during January–February, compared to 15% during 1999–2017 consistent with warming. Winter rainfall reduction is also responsible for shifting the spring soil moisture minimum to earlier in the year due to an earlier drying out of stored water content. Changes in winter precipitation in the decades we analyze are consistent with climate shifts in tropical Pacific SSTs.

5. Implications

Our study indicates that to date precipitation in the winter–spring has been the dominant mechanism impacting

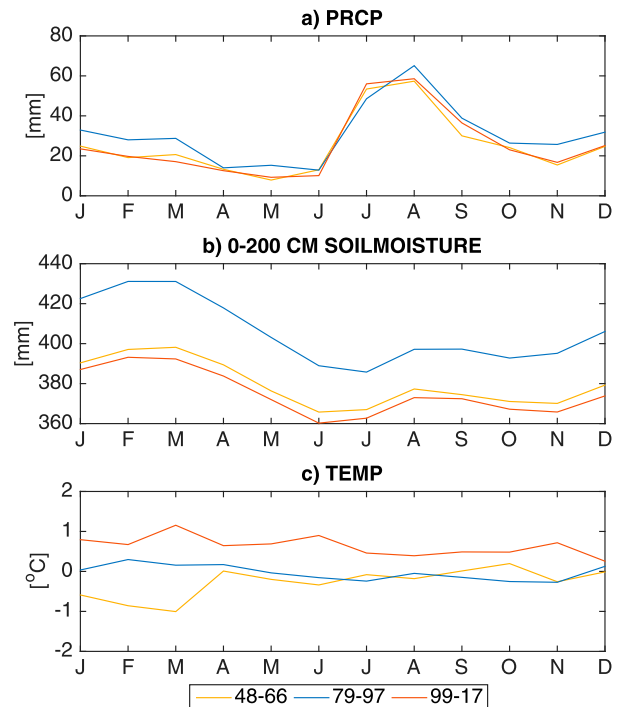


FIG. 13. Seasonal cycle of the bimodal region showing decadal shift of hydrological variables: (a) CLIMGRID precipitation, (b) soil moisture (SM-MCDI), and (c) CLIMGRID temperature seasonal cycle anomaly (anomaly based on 1948–2017 period). For each of the variables we plot the average seasonal cycle from wet decades (1979–97) and dry decades (the earlier dry period in 1948–66 and the later period in 1999–2017).

drying. Precipitation in turn is strongly associated with tropical Pacific SST, and future decadal variability of the Pacific will be critical for controlling the dynamics of the spring dry season in the future. Given the relationship between winter precipitation, soil moisture, and spring vegetation (Notaro et al. 2010; Vivoni et al. 2008; Robinson et al. 2013), future changes in winter precipitation due to the combined effects of natural decadal variability and emerging forced spring drying could have negative consequences on ecosystem productivity. Anthropogenic climate change in the SWUS is projected to intensify aridification (Seager et al. 2007), particularly during the spring (Gao et al. 2014; Ting et al. 2018).

Despite the dominant role of precipitation, we also detected a heightened role of temperature in the recent post 1999 drought compared to the midcentury drought. This has important implications in light of projected temperature increases. The influence of changes in precipitation will occur against a background of enhanced PET due to higher temperatures in the future. However, if due to natural variability, the tropical Pacific returns to warm or neutral conditions as has been forecast (e.g., Ramesh et al. 2017) then this would introduce a tendency

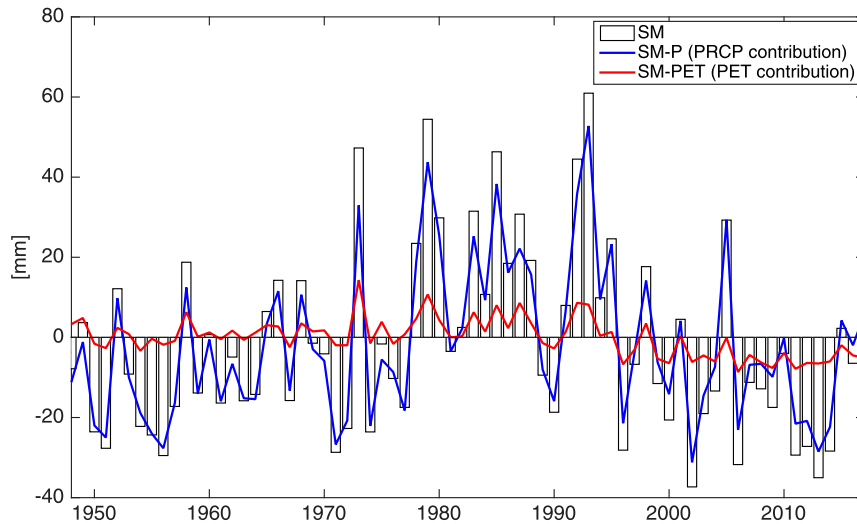


FIG. 14. Decomposition of spring (AMJ) soil moisture to show the contribution of PET (red line) and SM-P (blue line) to SM (bars) for the SWUS bimodal region. Anomalies are calculated based relative to the 1921–2000 mean.

to a wetter winter and a later onset and wetter spring dry season that would, at least temporarily, work against the human-driven trend toward drying.

Other impacts include the response of vegetation to CO_2 fertilization, in which increased amounts of atmospheric CO_2 enhance vegetation growth (Milly and Dunne 2016). Analyzing projections of the twenty-first century with an Earth system model, the SWUS was found to become both greener and drier (Mankin et al. 2017). Future research questions could focus on whether the model-projected enhanced spring drying will be offset by physiological effects of CO_2 on ecosystems in this region. Greater vegetation cover could also have the effect of enhancing water losses through ET in the spring and early summer, reducing soil moisture and runoff (Mankin et al. 2017, 2018).

A changing climate may also impact ecosystems in other indirect ways. Warming has contributed to greater outbreaks of bark beetles and wildfires in the western United States (Abatzoglou and Williams 2016; Westerling et al. 2006; Morgan et al. 2008; Raffa et al. 2008), both of which enhance tree mortality (Williams et al. 2013). Our study has found a reduction in moisture during the spring, in addition to warmer summer temperatures. Warming and reduced soil moisture increase the vapor pressure deficit (VPD), the difference between the water vapor content of the air and the saturation value, a quantity observed to correlate strongly to annual forest fire area in the western United States (Seager et al. 2015; Williams et al. 2015). Changes in moisture, temperature, and VPD could all increase susceptibility of trees to bark beetle infestation and wildfire in the future.

Finally, a reduction and advance in the timing of peak runoff in the spring due to earlier snowmelt has been identified for western rivers (Stewart et al. 2005; Regonda et al. 2005). Enhanced winter and spring drying in the future could also contribute to reduced and earlier streamflow peaks for this region, as suggested by observational studies on the increasing role of temperature (Woodhouse et al. 2016; Barnett et al. 2008), and future

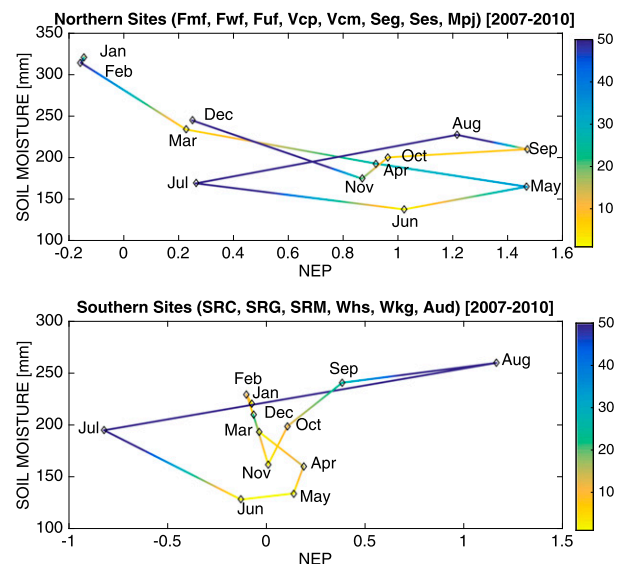


FIG. A1. Scatterplot of AmeriFlux NEP (x axis) plotted against 0–10-cm NLDAS-2 Noah soil moisture (y axis), and NLDAS-2 forcing precipitation (color bar shading) for northern sites (Fmf, Fwf, Fuf, Vcp, Vcm, Seg, Ses, Mpi) and southern sites (SRC, SRG, SRM, Whs, Wkg, Aud). The average seasonal cycle for the years 2007–10 is shown.

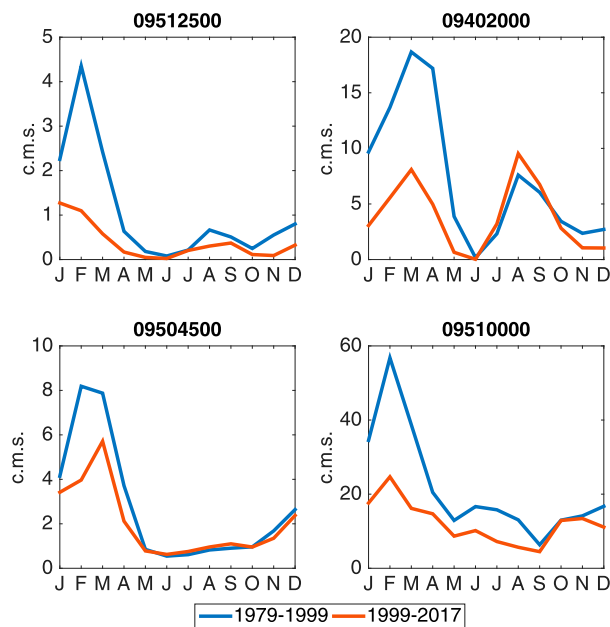


FIG. A2. Streamflow seasonal cycle showing decadal shift of wet decades (1979–97) and dry decades (1999–2017) for the following USGS gauges: 09512500, 09402000, 09504500, 09510000.

projections (Seager et al. 2013b; Barnett et al. 2008; Mankin et al. 2017; Ting et al. 2018). Reduced streamflow would be harmful to riparian ecosystems (Jaeger et al. 2014; Perkin and Gido 2011). River fragmentation is particularly deleterious to fish breeding, which rely on flowing waters as part of the spawning process, because of the impacts of fish being trapped in anoxic and stagnant river segments (Perkin and Gido 2011; Dudley and Platania 2007). Summer temperatures could potentially also lead to greater ET, reducing the summer streamflow peak in the future.

Given the sensitivity of this SWUS region to climate change, and the implications on ecosystems, wildfire, and streamflow, improved understanding of the mechanisms tying together the climate, hydrological, and ecological systems is important for explaining past and future environmental variability and change.

Acknowledgments. This work was supported by the National Science Foundation Graduate Research Fellowship award. The work was also supported by the NSF Award AGS-1243204 “Linking near-term future changes in weather and hydroclimate in western North America to adaptation for ecosystem and water management.” BIC, RS, and APW were also supported by the NASA Modeling, Analysis, and Prediction program (NASA 80NSSC17K0265). This work was also supported in part by the U.S. Army Corps of Engineers Climate Preparedness and Resilience Community of

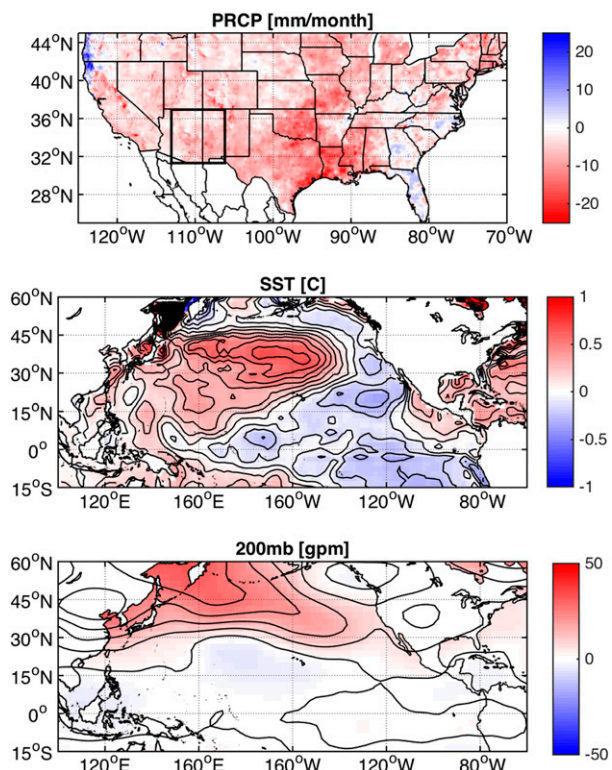


FIG. A3. Midcentury dry decades (1948–66) minus wet decades (1979–97) for (a) PRISM precipitation, (b) detrended NCEP–NCAR SST, and (c) NCEP–NCAR 200-mb geopotential heights. Contours are plotted at 0.25°C intervals for SST, and at 20-m intervals for geopotential height.

Practice. The views expressed are those of the author(s) and do not necessarily represent those of the U.S. Army Corps of Engineers. We thank the anonymous reviewers for their constructive criticisms.

APPENDIX

Additional Figures

This appendix contains Figs. A1–A3, which accompany the results of the article.

REFERENCES

Abatzoglou, J. T., and A. P. Williams, 2016: Impact of anthropogenic climate change on wildfire across western us forests. *Proc. Natl. Acad. Sci. USA*, **113**, 11 770–11 775, <https://doi.org/10.1073/pnas.1607171113>.

Adams, D. K., and A. C. Comrie, 1997: The North American Monsoon. *Bull. Amer. Meteor. Soc.*, **78**, 2197–2213, [https://doi.org/10.1175/1520-0477\(1997\)078<2197:TNAM>2.0.CO;2](https://doi.org/10.1175/1520-0477(1997)078<2197:TNAM>2.0.CO;2).

Arias, P. A., R. Fu, C. Vera, and M. Rojas, 2015: A correlated shortening of the North and South American monsoon seasons in the past few decades. *Climate Dyn.*, **45**, 3183–3203, <https://doi.org/10.1007/s00382-015-2533-1>.

- Ault, T. R., 2015: Trends and natural variability of spring onset in the coterminous United States as evaluated by a new gridded dataset of spring indices. *J. Climate*, **28**, 8363–8378, <https://doi.org/10.1175/JCLI-D-14-00736.1>.
- Baldocchi, D., and Coauthors, 2001: FLUXNET: A new tool to study the temporal and spatial variability of ecosystem-scale carbon dioxide, water vapor, and energy flux densities. *Bull. Amer. Meteor. Soc.*, **82**, 2415–2434, [https://doi.org/10.1175/1520-0477\(2001\)082<2415:FANTTS>2.3.CO;2](https://doi.org/10.1175/1520-0477(2001)082<2415:FANTTS>2.3.CO;2).
- Barnett, T. P., and Coauthors, 2008: Human-induced changes in the hydrology of the western United States. *Science*, **319**, 1080–1083, <https://doi.org/10.1126/science.1152538>.
- Breshears, D. D., and Coauthors, 2005: Regional vegetation die-off in response to global-change-type drought. *Proc. Natl. Acad. Sci. USA*, **102**, 15 144–15 148, <https://doi.org/10.1073/pnas.0505734102>.
- Castro, C. L., T. B. McKee, and R. A. Pielke, 2001: The relationship of the North American monsoon to tropical and North Pacific sea surface temperatures as revealed by observational analyses. *J. Climate*, **14**, 4449–4473, [https://doi.org/10.1175/1520-0442\(2001\)014<4449:TROTNA>2.0.CO;2](https://doi.org/10.1175/1520-0442(2001)014<4449:TROTNA>2.0.CO;2).
- Cayan, D. R., M. D. Dettinger, S. A. Kammerdiener, J. M. Caprio, and D. H. Peterson, 2001: Changes in the onset of spring in the Western United States. *Bull. Amer. Meteor. Soc.*, **82**, 399–415, [https://doi.org/10.1175/1520-0477\(2001\)082<0399:CITOOOS>2.3.CO;2](https://doi.org/10.1175/1520-0477(2001)082<0399:CITOOOS>2.3.CO;2).
- Cook, B. I., and R. Seager, 2013: The response of the North American Monsoon to increased greenhouse gas forcing. *J. Geophys. Res. Atmos.*, **118**, 1690–1699, <https://doi.org/10.1002/jgrd.50111>.
- , E. R. Cook, K. J. Anchukaitis, R. Seager, and R. L. Miller, 2011: Forced and unforced variability of twentieth century North American droughts and pluvials. *Climate Dyn.*, **37**, 1097–1110, <https://doi.org/10.1007/s00382-010-0897-9>.
- , T. R. Ault, and J. E. Smerdon, 2015: Unprecedented 21st century drought risk in the American Southwest and Central Plains. *Sci. Adv.*, **1**, e1400082, <https://doi.org/10.1126/sciadv.1400082>.
- Daly, C., M. Halbleib, J. I. Smith, W. P. Gibson, M. K. Doggett, G. H. Taylor, J. Curtis, and P. P. Pasteris, 2008: Physiographically sensitive mapping of climatological temperature and precipitation across the conterminous United States. *Int. J. Climatol.*, **28**, 2031–2064, <https://doi.org/10.1002/joc.1688>.
- Delworth, T. L., F. Zeng, A. Rosati, G. A. Vecchi, and A. T. Wittenberg, 2015: A link between the hiatus in global warming and North American drought. *J. Climate*, **28**, 3834–3845, <https://doi.org/10.1175/JCLI-D-14-00616.1>.
- Dore, S., and Coauthors, 2010: Carbon and water fluxes from ponderosa pine forests disturbed by wildfire and thinning. *Ecol. Appl.*, **20**, 663–683, <https://doi.org/10.1890/09-0934.1>.
- Dudley, R. K., and S. P. Platania, 2007: Flow regulation and fragmentation imperil pelagic-spawning riverine fishes. *Ecol. Appl.*, **17**, 2074–2086, <https://doi.org/10.1890/06-1252.1>.
- Enfield, D. B., A. Mestas-Nunez, and P. Trimble, 2001: The Atlantic Multidecadal Oscillation and its relation to rainfall and river flows in the continental U.S. *Geophys. Res. Lett.*, **28**, 2077–2080, <https://doi.org/10.1029/2000GL012745>.
- Fritze, H., I. T. Stewart, and E. Pebesma, 2011: Shifts in western North American snowmelt runoff regimes for the recent warm decades. *J. Hydrometeorol.*, **12**, 989–1006, <https://doi.org/10.1175/2011JHM1360.1>.
- Gao, Y., L. R. Leung, J. Lu, Y. Liu, M. Huang, and Y. Qian, 2014: Robust spring drying in the southwestern U.S. and seasonal migration of wet/dry patterns in a warmer climate. *Geophys. Res. Lett.*, **41**, 1745–1751, <https://doi.org/10.1002/2014GL059562>.
- Guirguis, K. J., and R. Avissar, 2008: A precipitation climatology and dataset intercomparison for the western United States. *J. Hydrometeorol.*, **9**, 825–841, <https://doi.org/10.1175/2008JHM832.1>.
- Hand, J. L., W. H. White, K. A. Gebhart, N. P. Hyslop, T. E. Gill, and B. A. Schichtel, 2016: Earlier onset of the spring fine dust season in the southwestern United States. *Geophys. Res. Lett.*, **43**, 4001–4009, <https://doi.org/10.1002/2016GL068519>.
- Higgins, R. W., and W. Shi, 2001: Intercomparison of the principal modes of interannual and intraseasonal variability of the North American Monsoon system. *J. Climate*, **14**, 403–417, [https://doi.org/10.1175/1520-0442\(2001\)014<0403:IOTPMO>2.0.CO;2](https://doi.org/10.1175/1520-0442(2001)014<0403:IOTPMO>2.0.CO;2).
- , Y. Chen, and A. V. Douglas, 1999: Interannual variability of the North American warm season precipitation regime. *J. Climate*, **12**, 653–680, [https://doi.org/10.1175/1520-0442\(1999\)012<0653:IVOTNA>2.0.CO;2](https://doi.org/10.1175/1520-0442(1999)012<0653:IVOTNA>2.0.CO;2).
- Hoerling, M. P., M. Dettinger, K. Wolter, J. Lukas, J. Eischeid, R. Nemani, B. Liebmann, and K. E. Kunkel, 2013: Present weather and climate: Evolving conditions. *Assessment of Climate Change in the Southwest United States: A Report Prepared for the National Climate Assessment*, G. Garfin et al., Eds., Island Press, 74–100.
- Huang, H.-P., R. Seager, and Y. Kushnir, 2005: The 1976/77 transition in precipitation over the Americas and the influence of tropical sea surface temperature. *Climate Dyn.*, **24**, 721–740, <https://doi.org/10.1007/s00382-005-0015-6>.
- Huxman, T. E., and Coauthors, 2004: Precipitation pulses and carbon fluxes in semiarid and arid ecosystems. *Oecologia*, **141**, 254–268, <https://doi.org/10.1007/s00442-004-1682-4>.
- Jaeger, K. L., J. D. Olden, and N. A. Pelland, 2014: Climate change poised to threaten hydrologic connectivity and endemic fishes in dryland streams. *Proc. Natl. Acad. Sci. USA*, **111**, 13 894–13 899, <https://doi.org/10.1073/pnas.1320890111>.
- Kalnay, E., M. Kanamitsu, R. Kistler, W. Collins, and D. Deaven, 1996: The NCEP/NCAR 40-Year Reanalysis Project. *Bull. Amer. Meteor. Soc.*, **77**, 437–471, [https://doi.org/10.1175/1520-0477\(1996\)077<0437:TNYRP>2.0.CO;2](https://doi.org/10.1175/1520-0477(1996)077<0437:TNYRP>2.0.CO;2).
- Kurc, S. A., and E. E. Small, 2007: Soil moisture variations and ecosystem-scale fluxes of water and carbon in semiarid grassland and shrubland. *Water Resour. Res.*, **43**, W06416, <https://doi.org/10.1029/2006WR005011>.
- Lehner, F., C. Deser, I. R. Simpson, and L. Terray, 2018: Attributing the U.S. Southwest’s recent shift into drier conditions. *Geophys. Res. Lett.*, **45**, 6251–6261, <https://doi.org/10.1029/2018GL078312>.
- Loik, M. E., D. D. Breshears, W. K. Lauenroth, and J. Belnap, 2004: A multi-scale perspective of water pulses in dryland ecosystems: climatology and ecohydrology of the western USA. *Oecologia*, **141**, 269–281, <https://doi.org/10.1007/s00442-004-1570-y>.
- Mankin, J. S., J. E. Smerdon, B. I. Cook, A. P. Williams, and R. Seager, 2017: The curious case of projected twenty-first-century drying but greening in the American West. *J. Climate*, **30**, 8689–8710, <https://doi.org/10.1175/JCLI-D-17-0213.1>.
- , R. Seager, J. E. Smerdon, B. I. Cook, A. P. Williams, and R. M. Horton, 2018: Blue water trade-offs with vegetation in a CO₂-enriched climate. *Geophys. Res. Lett.*, **45**, 3115–3125, <https://doi.org/10.1002/2018GL077051>.
- Mantua, N. J., S. R. Hare, Y. Zhang, J. M. Wallace, and R. C. Francis, 1997: A Pacific interdecadal climate oscillation with impacts on salmon production. *Bull. Amer. Meteor. Soc.*, **78**, 1069–1079, [https://doi.org/10.1175/1520-0477\(1997\)078<1069:APICOW>2.0.CO;2](https://doi.org/10.1175/1520-0477(1997)078<1069:APICOW>2.0.CO;2).

- Matsui, T., V. Lakshmi, and E. E. Small, 2005: The effects of satellite-derived vegetation cover variability on simulated land-atmosphere interactions in the NAMS. *J. Climate*, **18**, 21–40, <https://doi.org/10.1175/JCLI3254.1>.
- McCabe, G., M. Palecki, and J. Betancourt, 2004: Pacific and Atlantic Ocean influences on multidecadal drought frequency in the United States. *Proc. Natl. Acad. Sci. USA*, **101**, 4136–4141, <https://doi.org/10.1073/pnas.0306738101>.
- Mesinger, F., and Coauthors, 2006: North American Regional Reanalysis. *Bull. Amer. Meteor. Soc.*, **87**, 343–360, <https://doi.org/10.1175/BAMS-87-3-343>.
- Milly, P. C., and K. A. Dunne, 2016: Potential evapotranspiration and continental drying. *Nat. Climate Change*, **6**, 946–949, <https://doi.org/10.1038/nclimate3046>.
- Morgan, P., E. K. Heyerdahl, and C. E. Gibson, 2008: Multiseason climate synchronized forest fires throughout the 20th century, Northern Rockies, USA. *Ecology*, **89**, 717–728, <https://doi.org/10.1890/06-2049.1>.
- Mote, P. W., A. F. Hamlet, M. P. Clark, and D. P. Lettenmaier, 2005: Declining mountain snowpack in Western North America. *Bull. Amer. Meteor. Soc.*, **86**, 39–49, <https://doi.org/10.1175/BAMS-86-1-39>.
- , S. Li, D. P. Lettenmaier, M. Xiao, and R. Engel, 2018: Dramatic declines in snowpack in the western US. *npj Climate Atmos. Sci.*, **1**, 2, <https://doi.org/10.1038/s41612-018-0012-1>.
- Muldavin, E. H., D. I. Moore, S. L. Collins, K. R. Wetherill, and D. C. Lightfoot, 2008: Aboveground net primary production dynamics in a northern Chihuahuan desert ecosystem. *Oecologia*, **155**, 123–132, <https://doi.org/10.1007/s00442-007-0880-2>.
- Notaro, M., and D. Gutzler, 2012: Simulated impact of vegetation on climate across the North American monsoon region in CCSM3.5. *Climate Dyn.*, **38**, 795–814, <https://doi.org/10.1007/s00382-010-0990-0>.
- , Z. Liu, R. G. Gallimore, J. W. Williams, D. S. Gutzler, and S. Collins, 2010: Complex seasonal cycle of ecohydrology in the southwest United States. *J. Geophys. Res. Biogeosci.*, **115**, G04034, <https://doi.org/10.1029/2010JG001382>.
- Pascale, S., W. R. Boos, S. Bordoni, T. L. Delworth, S. B. Kapnick, H. Murakami, G. A. Vecchi, and W. Zhang, 2017: Weakening of the North American monsoon with global warming. *Nat. Climate Change*, **7**, 806–812, <https://doi.org/10.1038/nclimate3412>.
- Perkin, J. S., and K. B. Gido, 2011: Stream fragmentation thresholds for a reproductive guild of Great Plains fishes. *Fisheries*, **36**, 371–383, <https://doi.org/10.1080/03632415.2011.597666>.
- Raffa, K. F., B. H. Aukema, B. J. Bentz, A. L. Carroll, J. A. Hicke, M. G. Turner, and W. H. Romme, 2008: Cross-scale drivers of natural disturbances prone to anthropogenic amplification: The dynamics of bark beetle eruptions. *BioScience*, **58**, 501–517, <https://doi.org/10.1641/B580607>.
- Ramesh, N., M. A. Cane, R. Seager, and D. E. Lee, 2017: Predictability and prediction of persistent cool states of the Tropical Pacific Ocean. *Climate Dyn.*, **49**, 2291–2307, <https://doi.org/10.1007/s00382-016-3446-3>.
- Regonda, S. K., B. Rajagopalan, M. Clark, and J. Pitlick, 2005: Seasonal cycle shifts in hydroclimatology over the western United States. *J. Climate*, **18**, 372–384, <https://doi.org/10.1175/JCLI3272.1>.
- Robinson, T. M., K. J. La Pierre, M. A. Vadeboncoeur, K. M. Byrne, M. L. Thomey, and S. E. Colby, 2013: Seasonal, not annual precipitation drives community productivity across ecosystems. *Oikos*, **122**, 727–738, <https://doi.org/10.1111/j.1600-0706.2012.20655.x>.
- Ropelewski, C. F., and M. S. Halpert, 1986: North American precipitation and temperature patterns associated with the El Niño/Southern Oscillation (ENSO). *Mon. Wea. Rev.*, **114**, 2352–2362, [https://doi.org/10.1175/1520-0493\(1986\)114<2352:NAPATP>2.0.CO;2](https://doi.org/10.1175/1520-0493(1986)114<2352:NAPATP>2.0.CO;2).
- , and —, 1989: Precipitation patterns associated with the high index phase of the Southern Oscillation. *J. Climate*, **2**, 268–284, [https://doi.org/10.1175/1520-0442\(1989\)002<0268:PPAWTH>2.0.CO;2](https://doi.org/10.1175/1520-0442(1989)002<0268:PPAWTH>2.0.CO;2).
- Scott, R. L., G. D. Jenerette, D. L. Potts, and T. E. Huxman, 2009: Effects of seasonal drought on net carbon dioxide exchange from a woody-plant-encroached semiarid grassland. *J. Geophys. Res.*, **114**, G04004, <https://doi.org/10.1029/2008JG000900>.
- Seager, R., and G. A. Vecchi, 2010: Greenhouse warming and the 21st century hydroclimate of southwestern North America. *Proc. Natl. Acad. Sci. USA*, **107**, 21 277–21 282, <https://doi.org/10.1073/pnas.0910856107>.
- , Y. Kushnir, C. Herweijer, N. Naik, and J. Velez, 2005: Modeling of tropical forcing of persistent droughts and pluvials over western North America: 1856–2000. *J. Climate*, **18**, 4065–4088, <https://doi.org/10.1175/JCLI3522.1>.
- , M. Ting, I. Held, Y. Kushnir, and J. Lu, 2007: Model projections of an imminent transition to a more arid climate in southwestern North America. *Science*, **316**, 1181–1184, <https://doi.org/10.1126/science.1139601>.
- , —, C. Li, N. Naik, B. Cook, J. Nakamura, and H. Liu, 2013a: Projections of declining surface-water availability for the southwestern United States. *Nat. Climate Change*, **3**, 482–486, <https://doi.org/10.1038/nclimate1787>.
- , —, —, —, —, —, and —, 2013b: Projections of declining surface-water availability for the southwestern United States. *Nat. Climate Change*, **3**, 482–486, <https://doi.org/10.1038/nclimate1787>.
- , A. Hooks, A. P. Williams, B. Cook, J. Nakamura, and N. Henderson, 2015: Climatology, variability, and trends in the U.S. vapor pressure deficit, an important fire-related meteorological quantity. *J. Appl. Meteor. Climatol.*, **54**, 1121–1141, <https://doi.org/10.1175/JAMC-D-14-0321.1>.
- Sheffield, J., G. Goteti, and E. F. Wood, 2006: Development of a 50-year high-resolution global dataset of meteorological forcings for land surface modeling. *J. Climate*, **19**, 3088–3111, <https://doi.org/10.1175/JCLI3790.1>.
- Small, E. E., 2001: The influence of soil moisture anomalies on variability of the North American Monsoon System. *Geophys. Res. Lett.*, **28**, 139–142, <https://doi.org/10.1029/2000GL011652>.
- Stewart, I. T., D. Cayan, and M. D. Dettinger, 2005: Changes toward earlier streamflow timing across western North America. *J. Climate*, **18**, 1136–1155, <https://doi.org/10.1175/JCLI3321.1>.
- Sullivan, B. W., T. E. Kolb, S. C. Hart, J. P. Kaye, B. A. Hungate, S. Dore, and M. Montes-Helu, 2011: Wildfire reduces carbon dioxide efflux and increases methane uptake in ponderosa pine forest soils of the southwestern USA. *Biogeochemistry*, **104**, 251–265, <https://doi.org/10.1007/s10533-010-9499-1>.
- Ting, M., R. Seager, C. Li, H. Liu, and N. Henderson, 2018: Mechanism of future spring drying in the southwest U.S. in CMIP5 models. *J. Climate*, **31**, 4265–4279, <https://doi.org/10.1175/JCLI-D-17-0574.1>.
- Tucker, C. J., J. E. Pinzon, M. E. Brown, and E. Molly, 2004: Global inventory modeling and mapping studies (GIMMS) satellite drift corrected and NOAA-16 incorporated Normalized Difference Vegetation Index (NDVI), monthly 1981–2002. Global Land Cover Facility, University of Maryland, College Park, accessed November 2016, https://iridl.ldeo.columbia.edu/SOURCES/UMD/GLCF/GIMMS/NDVI/global/dataset_documentation.html.

- Vivoni, E. R., H. A. Moreno, G. Mascaro, J. C. Rodriguez, C. J. Watts, J. Garatuza-Payan, and R. L. Scott, 2008: Observed relation between evapotranspiration and soil moisture in the North American monsoon region. *Geophys. Res. Lett.*, **35**, L22403, <https://doi.org/10.1029/2008GL036001>.
- Vose, R. S., and Coauthors, 2014: Improved historical temperature and precipitation time series for U.S. climate divisions. *J. Appl. Meteor. Climatol.*, **53**, 1232–1251, <https://doi.org/10.1175/JAMC-D-13-0248.1>.
- Watts, C. J., R. L. Scott, J. Garatuza-Payan, J. C. Rodriguez, J. H. Prueger, W. P. Kustas, and M. Douglas, 2007: Changes in vegetation condition and surface fluxes during NAME 2004. *J. Climate*, **20**, 1810–1820, <https://doi.org/10.1175/JCLI4088.1>.
- Westerling, A. L., H. G. Hidalgo, D. R. Cayan, and T. W. Swetnam, 2006: Warming and earlier spring increase western U.S. forest wildfire activity. *Science*, **313**, 940–943, <https://doi.org/10.1126/science.1128834>.
- Williams, A. P., and Coauthors, 2013: Temperature as a potent driver of regional forest drought stress and tree mortality. *Nat. Climate Change*, **3**, 292–297, <https://doi.org/10.1038/nclimate1693>.
- , and Coauthors, 2014: Causes and implications of extreme atmospheric moisture demand during the record-breaking 2011 wildfire season in the southwestern United States. *J. Appl. Meteor. Climatol.*, **53**, 2671–2684, <https://doi.org/10.1175/JAMC-D-14-0053.1>.
- , and Coauthors, 2015: Correlations between components of the water balance and burned area reveal new insights for predicting forest fire area in the southwest United States. *Int. J. Wildland Fire*, **24**, 14–26, <https://doi.org/10.1071/WF14023>.
- , B. I. Cook, J. E. Smerdon, D. A. Bishop, R. Seager, and J. S. Mankin, 2017: The 2016 southeastern U.S. drought: An extreme departure from centennial wetting and cooling. *J. Geophys. Res. Atmos.*, **122**, 10 888–10 905, <https://doi.org/10.1002/2017JD027523>.
- Woodhouse, C. A., G. T. Pederson, K. Morino, S. A. McAfee, and G. J. McCabe, 2016: Increasing influence of air temperature on upper Colorado River streamflow. *Geophys. Res. Lett.*, **43**, 2174–2181, <https://doi.org/10.1002/2015GL067613>.
- Xia, Y., and Coauthors, 2012: Continental-scale water and energy flux analysis and validation for the North American Land Data Assimilation System project phase 2 (NLDAS-2): 1. Intercomparison and application of model products. *J. Geophys. Res.*, **117**, D03109, <https://doi.org/10.1029/2011JD016048>.
- Zhang, Y., J. M. Wallace, and D. S. Battisti, 1997: ENSO-like interdecadal variability: 1900–93. *J. Climate*, **10**, 1004–1020, [https://doi.org/10.1175/1520-0442\(1997\)010<1004:ELIV>2.0.CO;2](https://doi.org/10.1175/1520-0442(1997)010<1004:ELIV>2.0.CO;2).